

Out-of-plane bond order phase, superconductivity, and their competition in the t - J_{\parallel} - J_{\perp} model for pressurized nickelates

Matías Bejas,¹ Xianxin Wu,² Debmalya Chakraborty,³ Andreas P. Schnyder,⁴ and Andrés Greco^{1,4}

¹*Facultad de Ciencias Exactas, Ingeniería y Agrimensura and Instituto de Física Rosario (UNR-CONICET), Avenida Pellegrini 250, 2000 Rosario, Argentina*

²*Institute for Theoretical Physics, Chinese Academy of Sciences, Beijing, China*

³*Max Planck Institute for the Physics of Complex Systems, Nöthnitzer Straße 38, 01187, Dresden, Germany*

⁴*Max Planck Institute for Solid State Research, Heisenbergstrasse 1, 70569 Stuttgart, Germany*

(Dated: November 4, 2024)

Almost four decades of intense research have been invested to study the physics of high- T_c cuprate superconductors. The recent discovery of high- T_c superconductivity in pressurized bilayer nickelates and its potential similarities with cuprate superconductors may open a new window to understand this long standing problem. Motivated by this we have assumed that nickelates belong to the category of strongly correlated systems, and considered the bilayer t - J_{\parallel} - J_{\perp} model as a minimal model, where J_{\parallel} and J_{\perp} are the in-plane and out-of-plane magnetic exchange, respectively. We have studied the t - J_{\parallel} - J_{\perp} model in a large- N approach on the basis of the path integral representation for Hubbard operators, which allows to obtain results at mean-field and beyond mean-field level. We find that J_{\perp} is a promising candidate for triggering high superconducting T_c values at quarter filling (hole doping $\delta = 0.5$) of the $d_{x^2-y^2}$ orbitals. Beyond mean-field level, we remarkably find a new phase, an out-of-plane bond-order phase (z-BOP), triggered also by J_{\perp} . z-BOP develops below a critical temperature which decreases with increasing doping and vanishes at a quantum critical point below quarter filling. The occurrence of this phase and its competition with superconductivity leads to a superconducting dome shaped behavior as a function of doping and as a function of J_{\perp} . Comparisons with the physics of cuprates and the recent literature on the new pressurized nickelates are given along the paper.

I. INTRODUCTION

The recent discovery of superconductivity in the bilayer nickelates $\text{La}_3\text{Ni}_3\text{O}_7$ at high critical temperature $T_c \sim 80$ K [1, 2] under moderate pressure of about 14 GPa has motivated a huge experimental [3–21] and theoretical [22–48] interest. We have cited only part of the vast existing literature; see also [49] for a review. Trilayer pressurized $\text{La}_4\text{Ni}_3\text{O}_{10}$ nickelates have been also studied, and a lower value of T_c ($T_c \sim 30$ K) was obtained [4, 5, 13, 15, 21].

The experiments are not straightforward, because they are done at high pressure, such that the nature of the observed superconductivity has become subject of a debate [50]. For instance, in bilayer nickelates the volume fraction for superconductivity was primarily estimated experimentally to be of the order of 1% [9], and while some experiments reported zero residual resistance [2, 11, 20, 51] others did not [1, 8, 9]. Based on that situation, it was assumed that a filamentary superconductivity occurs in this material [8, 9]. Instead, trilayer nickelates shows about 80% of volume fraction for superconductivity [15]. However, recently the situation seems to have substantially changed. A volume fraction for superconductivity of about 50% and zero residual resistance were reported [51] in bilayer nickelates. The substitutions of Pr for La are found to effectively inhibit the intergrowth of different phases and result in a nearly pure bilayer structure, leading to bulk high T_c superconductivity in $\text{La}_2\text{PrNi}_2\text{O}_7$ [52]. In addition, the superconduct-

ing Meissner effect was very recently detected [53]. These findings, together with the high superconducting volume fraction in trilayer nickelates, might locate the new pressurized nickelates inside the category of bulk high- T_c superconductors as cuprates. In addition, in Ref. [51] the existence of a dome for T_c as a function of pressure was reported. That is, T_c increases with pressure reaching the maximum at 18 GPa, and for larger pressure T_c decreases.

For almost four decades cuprates superconductors were extensively investigated motivated by their high value of T_c and their anomalous properties, such as the pseudogap, strange metal phase, charge orders, and other features [54–58]. It is widely considered that cuprates superconductors are prototype materials for understanding correlated systems [59]. Through the years many systems had been studied such as, for instance, organic materials [60], cobaltates [61], iron superconductors [62], and more recently the kagome materials [63]. In all of them the possible contact with the physics of cuprates is discussed, although their T_c is much smaller.

There are close similarities between nickelates and cuprate superconductors [64]. Nickelates are formed by NiO_2 planes, where Ni is a neighbor of Cu in the periodic table, there is a presence of correlated Ni- d orbitals, and a high value of T_c . Then, it is very probable that the discovery of superconductivity in pressurized nickelates opens a new and promising window to look at the topic from another perspective. Several effective models have been proposed for nickelates, which

run from multi-orbitals (d_{z^2} and $d_{x^2-y^2}$) [12, 27, 28, 31–33, 39, 40, 42, 43, 45] to only one active quarter filling orbital $d_{x^2-y^2}$ [30, 35, 36] models.

Motivated by the analogies with high- T_c cuprates and strong coupling between NiO_2 layers through the inner apical oxygen, the strongly correlated t - J_{\parallel} - J_{\perp} [35–37] model is a promising candidate to describe the physics of bilayer nickelates $\text{La}_3\text{Ni}_3\text{O}_7$, where J_{\parallel} and J_{\perp} are the in-plane and out-of-plane magnetic exchanges, respectively. This is a minimal model where only the $d_{x^2-y^2}$ orbital plays an active role. It is formed by a t - t' - J_{\parallel} model for each plane as in cuprates [65] coupled by an out-of-plane J_{\perp} between planes. In addition, a small electron hopping t_{\perp} between planes is expected [35, 43]. This model was also discussed in the context of the slave boson approach at mean-field level [35], the density matrix renormalization group and infinite projected entangled-pair states [36].

In the present paper we study the t - J_{\parallel} - J_{\perp} model in a large- N approximation on the basis of the path integral representation [66, 67] for Hubbard operators [68], and perform calculations at mean-field and beyond mean-field level. We find robust tendencies to an out-of-plane s -wave superconductivity in the model which is triggered by J_{\perp} ; only if J_{\perp} is larger than a certain minimum value. Notably, we also obtain an out-of-plane bond order phase (z-BOP) instability below a critical temperature $T_c^{\text{z-BOP}}$ which decreases with increasing the doping δ ending at $T = 0$ at a quantum critical point (QCP) below quarter filling ($\delta = 0.5$). We study the competition between the z-BOP and superconductivity, and find a dome behavior for superconducting T_c at $\delta < 0.5$. We also discuss the possible role of z-BOP for the dome behavior for T_c as a function of pressure.

The paper is organized as following. In Sec. II we present generic theoretical results. Section III makes possible contact with the phenomenology of pressurized nickelates. In Sec. IV we present the conclusion and discussions.

II. GENERIC THEORETICAL RESULTS

A. The model and superconductivity due to J_{\perp}

As a minimal model we study the bilayer t - J_{\parallel} - J_{\perp} model [35, 36], where only the $d_{x^2-y^2}$ orbitals are considered active

$$\begin{aligned}
 H = & \sum_{i,j,\sigma,\alpha} t_{ij} \tilde{c}_{i\sigma,\alpha}^{\dagger} \tilde{c}_{j\sigma,\alpha} + J_{\parallel} \sum_{i,j,\alpha} \left(\vec{S}_{i,\alpha} \cdot \vec{S}_{j,\alpha} - \frac{1}{4} n_{i,\alpha} n_{j,\alpha} \right) \\
 & + \frac{J_{\perp}}{2} \sum_{i,\alpha} \left(\vec{S}_{i,\alpha} \cdot \vec{S}_{i,\bar{\alpha}} - \frac{1}{4} n_{i,\alpha} n_{i,\bar{\alpha}} \right) \\
 & + t_{\perp} \sum_{i,\sigma,\alpha} \tilde{c}_{i\sigma,\alpha}^{\dagger} \tilde{c}_{i\sigma,\bar{\alpha}} - \mu \sum_{i,\alpha} n_{i,\alpha}. \quad (1)
 \end{aligned}$$

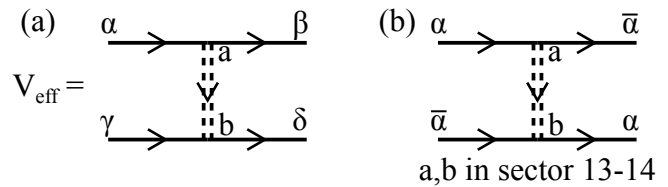


FIG. 1. (a) General superconducting effective interaction between fermions mediated by the full 14×14 bosonic propagator D_{ab} [Eq. (A25)]. (b) Out-of-plane superconducting effective interaction mediated by the bosonic propagator corresponding to the J_{\perp} subsector r_{\perp} - A_{\perp} [Eq. (B9)].

This one orbital bilayer model is derived from the bilayer two orbitals ($d_{x^2-y^2}$ and d_{z^2}) model in the limit of strong Hund's coupling J_H [35, 36]. In addition, $J_{\perp} > J_{\parallel}$ is discussed. A similar model was discussed in mean-field slave boson calculation in the context of magnetic excitations in bilayer cuprates [69]. In this work, an opposite regime to the one here was discussed, namely low doping and not focusing on the effects of J_{\perp} on superconductivity ($J_{\perp} \ll J_{\parallel}$).

In Eq. (1) α runs over the planes 1 and 2, $\bar{\alpha}$ represents the plane opposite to α , and i and j run over the sites of the square lattice of each plane. The hopping t_{ij} takes a value t between the first nearest-neighbors and t' between the next nearest-neighbors sites on each plane, μ is the chemical potential. The exchange interaction J_{\parallel} , takes a value between the first nearest-neighbor sites on each plane. The exchange interaction and the hopping integral between planes are J_{\perp} and t_{\perp} , respectively. $\tilde{c}_{i\sigma,\alpha}^{\dagger}$ ($\tilde{c}_{i\sigma,\alpha}$) is the creation (annihilation) operator of electrons in site i of the plane α with spin σ ($=\uparrow, \downarrow$) in the Fock space without double occupancy. $n_{i,\alpha} = \sum_{\sigma} \tilde{c}_{i\sigma,\alpha}^{\dagger} \tilde{c}_{i\sigma,\alpha}$ is the electron density operator and $\vec{S}_{i,\alpha}$ is the spin operator. For a given filling δ we compute the corresponding chemical potential μ in a self-consistent manner, as discussed in Appendix A, which also contains a complete description of the path integral large- N formulation of our model (1). In Sec. III we will argue that our model (1) at quarter filling $\delta = 0.5$ describes some of the essential physics of the bilayer nickelate $\text{La}_3\text{Ni}_3\text{O}_7$.

The general superconducting effective interaction between a fermion with momentum \mathbf{k} and energy ν_n and other with momentum \mathbf{k}' and energy ν'_n , $V_{\text{eff}}(\mathbf{k}, \mathbf{k}'; \nu_n, \nu'_n)$, can be calculated using the diagram in Fig. 1(a), which shows that in the present theory pairing is mediated by the 14×14 bosonic propagator D_{ab} [Eq. (A25)] formed by the 14-component bosonic field defined as [Eq. (A14)]:

$$\begin{aligned}
 \delta X^a = & (\delta R_1, \delta \lambda_1, \delta R_2, \delta \lambda_2, r_1^x, r_1^y, A_1^x, A_1^y, \\
 & r_2^x, r_2^y, A_2^x, A_2^y, r_{\perp}, A_{\perp}), \quad (2)
 \end{aligned}$$

where δR_{α} describes fluctuations of the number of holes at a given site in the plane α and it is related to on-site charge fluctuations in each plane, $\delta \lambda_{\alpha}$ is the fluctua-

tion of the Lagrange multiplier introduced to enforce the constraint that prohibits the double occupancy at any site in each plane, and r_α^x and r_α^y (A_α^x and A_α^y) describe fluctuations of the real (imaginary) part of the in-plane bond field coming from the J_\parallel -term. r_\perp and A_\perp are the real and imaginary part, respectively, of the out-of-plane bond field coming from the J_\perp -term. See Appendix A for technical details.

The analytical expression for the effective interaction is

$$V_{\text{eff}}(\mathbf{k}, \mathbf{k}'; \nu_n, \nu'_n) = \Lambda_{\alpha\beta,a} D_{ab}(\mathbf{k} - \mathbf{k}', \nu_n - \nu'_n) \Lambda_{\gamma\delta,b}, \quad (3)$$

where $\Lambda_{\alpha\beta,a}$ and $\Lambda_{\gamma\delta,b}$ are three-leg vertices [Eq. (A20) and Eq. (A21)] describing the interactions between fermions and bosons, where its momentum and frequency dependence are omitted for simplicity. The indices α, β, γ , and δ indicate the plane index (1 or 2), and the indices a and b the boson flavour [Eq. (2)]. Note that we can also draw a diagram containing two four-legs vertices $\Lambda_{\alpha\beta,ab}$ [Eq. (A22)] and two bosonic propagators D_{ab} , however, this contribution is omitted because it is $O(1/N^2)$.

In Appendix B we focus on the J_\perp -subspace of the full formulation. This is mainly motivated by the fact that in first approximation the J_\perp -sector of the 14×14 matrix D_{ab} [Eq. (A25)] contains the main topic of interest, i.e., J_\perp . In Fig. 1(b) we show the diagram for the out-of-plane effective interactions corresponding to the exchange term J_\perp of Eq. (1), i.e., sector 13-14 (also called r_\perp - A_\perp sector) of Eq. (2). Using the bare bosonic propagator [Eq. (B1)], which is equivalent to a mean-field calculation [70], and the three-leg vertices [Eq. (B2)], it is straightforward to show that the effective superconducting interaction from Fig. 1(b) reads as:

$$V_\perp^{\text{eff}}(\mathbf{k}, \mathbf{k}') = \frac{J_\perp}{4}, \quad (4)$$

which is clearly isotropic s -wave and unretarded. This result is consistent with the slave-boson mean-field approach [35] where the pairing strength is $\sim J_\perp$.

Similarly, the main in-plane contribution to superconductivity is given by the d -wave unretarded effective interaction [70]

$$V_\parallel^{\text{eff}}(\mathbf{k}, \mathbf{k}') = J_\parallel \gamma_d(\mathbf{k}) \gamma_d(\mathbf{k}'), \quad (5)$$

with $\gamma_d(\mathbf{k}) = \frac{1}{2}(\cos k_x - \cos k_y)$. This result can also be obtained in the present approach (Appendix A) if we focus on the in-plane J_\parallel -sector, i.e., the sector 1-12 of [Eq. (2)]. We note that the presence of unretarded effective interactions, also known as pairing without glue, in cuprates is still under discussion [70–73].

The presence of $V_\parallel^{\text{eff}}(\mathbf{k}, \mathbf{k}')$ and $V_\perp^{\text{eff}}(\mathbf{k}, \mathbf{k}')$ indicates the possibility of in- and out-of-plane superconductivity, respectively, and their interaction. In Appendix C we present the corresponding two-gap formulation, where the equations for the superconducting in-plane Δ_\parallel and out-of-plane Δ_\perp gaps, Eq. (C3) and Eq. (C4) respectively, are coupled to each other. In this paper, we

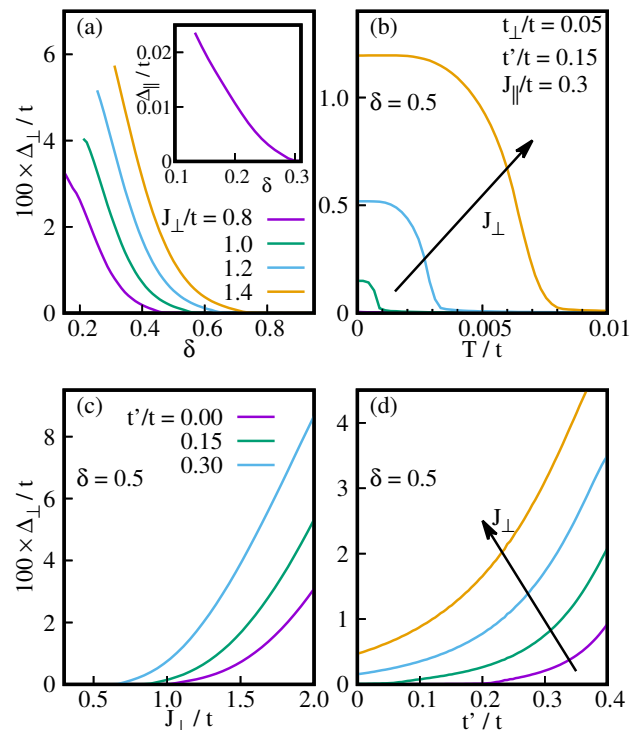


FIG. 2. Superconductivity in the bilayer t - J_\parallel - J_\perp model. (a) Out-of-plane superconducting gap Δ_\perp versus δ for $J_\perp/t = 0.8, 1.0, 1.2, 1.4$. (b) Δ_\perp versus T for $J_\perp/t = 1.0, 1.2, 1.4$ at $\delta = 0.50$. (c) Δ_\perp versus J_\perp for $t'/t = 0, 0.15, 0.3$ at $\delta = 0.5$. (d) Δ_\perp versus t' for $J_\perp/t = 0.8, 1.0, 1.2, 1.4$ at $\delta = 0.5$. The inset in (a) shows the in-plane superconducting gap Δ_\parallel versus δ for $J_\parallel/t = 0.3$ and $J_\perp = 0$ at $T = 0$.

present results for $J_\parallel/t = 0.3$ similar to cuprates [54] and $t_\perp/t = 0.05$ [35], while we vary t' , J_\perp , δ and the temperature T .

In Fig. 2(a) we plot the out-of-plane superconducting gap Δ_\perp versus doping for $J_\perp/t = 0.8, 1.0, 1.2$, and 1.4 , at $T = 0$. We obtain a robust out-of-plane s -wave superconductivity triggered by J_\perp for all dopings. Note that in spite of $J_\parallel/t = 0.3$, in Fig. 2(a) the in-plane $\Delta_\parallel = 0$ for all dopings, i.e., J_\perp disfavors in-plane d -wave superconductivity, as was also discussed in [37]. For completeness in the inset of Fig. 2(a) we show results for $J_\perp = 0$. Since $J_\parallel/t = 0.3$ is a condition similar to cuprates we obtain in-plane d -wave superconductivity. In fact, we show an in-plane Δ_\parallel gap versus doping which vanishes for doping $\delta \gtrsim 0.3$ as observed in cuprates [54]. Thus, it is clear that we cannot expect a large value for T_c at quarter filling ($\delta = 0.5$), unless we use unrealistic values for $J_\parallel/t \sim 2$. Besides, this value for J_\parallel is unrealistic, it triggers several instabilities, including phase separation, that may cover mainly the full phase diagram [74]. This shows that J_\perp is a potential candidate for triggering high T_c values at quarter filling in bilayer nickelates. The fact that the in-plane d -wave superconductivity triggered by J_\parallel is far from the doping of interest for pressurized nick-

elates justifies that in first approximation $V_{\parallel}^{\text{eff}}$ from the J_{\parallel} -sector can be studied separately from the J_{\perp} -sector. In Fig. 2(b), for $\delta = 0.5$, we plot Δ_{\perp} for $J_{\perp} = 1.0, 1.2$, and 1.4 versus temperature, and obtain the superconducting critical temperatures $T_c/t \sim 0.001, 0.003$, and 0.007, respectively. In agreement with Fig. 2(a) there is no superconductivity for $J_{\perp}/t = 0.8$ at quarter filling.

In Fig. 2(c) we show Δ_{\perp} versus J_{\perp} for $\delta = 0.5$, and $t'/t = 0, 0.15$, and 0.3. The figure shows that the superconducting gap at quarter filling, and the corresponding T_c , increases with increasing J_{\perp} and it is only expected for J_{\perp}/t bigger than a given value that decrease with increasing t' . The in-plane d -wave superconducting gap is $\Delta_{\parallel} = 0$ for all J_{\perp} in spite of $J_{\parallel}/t = 0.3$, which is due to the large doping value $\delta = 0.5$. A reasonable variation of t_{\perp} will not effectively affect Δ_{\perp} . However, a large t_{\perp} , comparable to J_{\perp} , will suppress Δ_{\perp} due to the Pauli blocking effect [36]. In Fig. 2(d) we show that Δ_{\perp} also increases with increasing the in-plane t' for all values of J_{\perp} chosen. In summary, tendencies to out-of-plane s -wave superconductivity increase with increasing J_{\perp} and t' , and in addition there is a lower limit for J_{\perp} below which superconductivity can not be expected.

B. Out-of-plane bond order phase z-BOP

In this section, we now investigate the instability in the charge channel. In particular, we focus on an out-of-plane bond order (z-BOP). For discussing the z-BOP we focus on the r_{\perp} - A_{\perp} sector of the matrix D_{ab} , i.e., the dressed $D_{z\text{-BOP}}$ [Eq. (B9)] which is beyond mean field level. When for a given doping, temperature $T_c^{\text{z-BOP}}$, and momentum \mathbf{q}_c , one eigenvalue of $D_{z\text{-BOP}}^{-1}$ is zero, the out-of-plane bond order instability takes place.

In Fig. 3 (a) we show $T_c^{\text{z-BOP}}$ versus doping for different values of J_{\perp} and t' . Clearly, with increasing J_{\perp} and t' the z-BOP expands its area in the phase diagram. Instead, z-BOP is nearly independent of t_{\perp} (not shown). In all cases $T_c^{\text{z-BOP}}$ decreases with increasing doping ending at a QCP at $T = 0$. The critical momentum \mathbf{q}_c is incommensurate and of the form $\mathbf{q}_c = (1, q)\pi$, with $q \sim 0.55\text{-}0.70$ at $T = 0$, and moves towards $\mathbf{q}_c = (\pi, \pi)$ with increasing T at lower dopings [see Fig. 3(d)]. Thus, below $T_c^{\text{z-BOP}}$ the z-BOP is the stable phase.

We note that for the present parameters the z-BOP occurs at much larger doping than the flux phase [74–77], or d CDW [78–81], in the two-dimensional (2D) t - J model. For instance, for $J_{\parallel}/t = 0.3$, and $t' = 0$, while for $J_{\perp} = 0$ the flux phase occurs at $\delta \lesssim 0.13$ at $T = 0$ [74, 77], the z-BOP for $J_{\perp}/t = 0.8$ occurs at $\delta \lesssim 0.24$. This fact justifies, in first approximation, the study of the z-BOP from the J_{\perp} -sector separately because it is relevant in the doping regime of our main interest, i.e., $\delta \sim 0.5$.

However, we have to take care close to half-filling and low temperature. While at $\delta = 0$, $T_c^{\text{z-BOP}} = J_{\perp}/8$ [see the points on the y -axis in Fig. 3(a)], the bond order in-

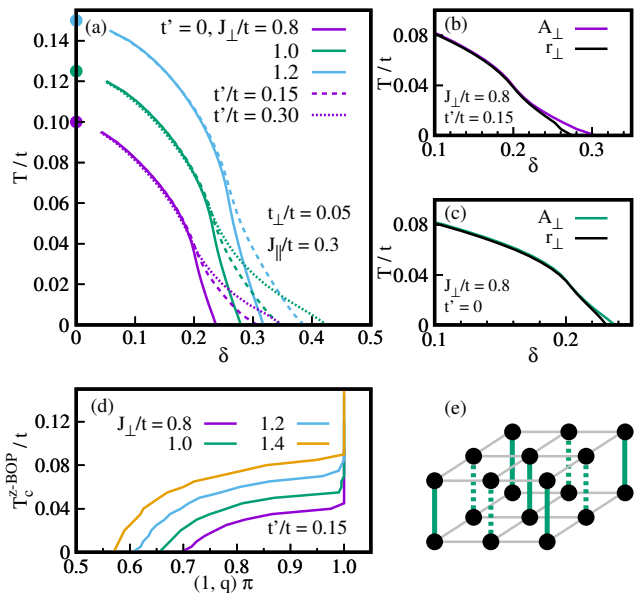


FIG. 3. (a) $T_c^{\text{z-BOP}}$ versus doping for different values of J_{\perp} and t' . The points on the y -axis are located at $J_{\perp}/8$ where each $T_c^{\text{z-BOP}}$ extrapolates to half-filling ($\delta = 0$). (b) $T_c^{\text{z-BOP}}$, for both sectors r_{\perp} and A_{\perp} , for $J_{\perp}/t = 0.8$ and $t'/t = 0.15$. (c) The same as (b) but for $t' = 0$. (d) Temperature dependence of \mathbf{q}_c for $t'/t = 0.15$ and $J_{\perp}/t = 0.8, 1.0, 1.2, 1.4$. (e) Sketch of the z-BOP where the out-of-plane bonds are frozen following a pattern with ordered momentum $\mathbf{q}_c = (\pi, \pi)$.

stabilities, including the flux phase, in the pure 2D t - J model develops at $T = J_{\parallel}/8$ [74]. Then, at low doping and low T a competition between the 2D bond order instabilities and z-BOP is expected. Such analysis requires the full approach (Appendix A), which is a big challenge that demands the stability analysis of the 14×14 D_{ab} matrix and deserves a separate theoretical study.

The leading instability of the z-BOP occurs in the sector A_{\perp} , i.e., the associated eigenvector of $D_{z\text{-BOP}}^{-1}$ [Eq. (B9)] is of the form $(0, 1)$. However, the instability in the sector r_{\perp} is very close and even both merge at high temperature, as can be seen in Fig. 3(b) and (c). Thus, the instabilities in the r_{\perp} and A_{\perp} sector are nearly degenerated. In addition, with decreasing t' the instabilities in both channels are even closer at $T = 0$, as can be seen by comparing results for $J_{\perp}/t = 0.8$ for $t'/t = 0.15$ [Fig. 3(b)] and $t' = 0$ [Fig. 3(c)].

The projection of $D_{z\text{-BOP}}$ on the two eigenvectors $(1, 0)$ and $(0, 1)$ leads to the z-BOP susceptibilities $\chi_{z\text{-BOP}}^{r_{\perp}}$ and $\chi_{z\text{-BOP}}^{A_{\perp}}$, Eq. (D1) and Eq. (D2), respectively. Thus, beyond mean-field level the out-of-plane bond susceptibilities diverge at a temperature $T_c^{\text{z-BOP}}$ and momentum \mathbf{q}_c .

In Fig. 4(a) we show the real part of the inverse of the static $[\chi_{z\text{-BOP}}^{r_{\perp}, A_{\perp}}(\mathbf{q}, \omega = 0)]$ z-BOP susceptibilities for $J_{\perp}/t = 0.8$ at $\delta \sim 0.31$ close to the QCP [Fig. 3(b)], and momentum \mathbf{q} along the $(\pi, 0)$ - (π, π) direction where the instability takes place. As it can be seen the susceptibil-

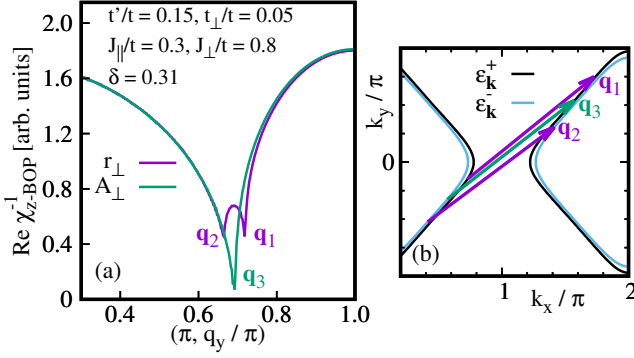


FIG. 4. (a) The inverse of the static z-BOP susceptibilities $\chi_{z\text{-BOP}}^{r_{\perp}}$ and $\chi_{z\text{-BOP}}^{A_{\perp}}$ along the $(\pi, 0)$ - (π, π) direction. (b) \mathbf{q}_1 and \mathbf{q}_2 are the two intra-band nesting wave-vectors associated with the two peaks of $\chi_{z\text{-BOP}}^{r_{\perp}}$, while \mathbf{q}_3 corresponds to inter-band nesting wave-vector associated with the single peak in $\chi_{z\text{-BOP}}^{A_{\perp}}$.

ities show strong peaks close to the incommensurate momentum $\mathbf{q}_c \sim (\pi, 0.7\pi)$ [see also Fig. 3(d)]. When these peaks reach the zero value the instability occurs. We can further ask: what is the origin of the z-BOP instability? The origin lies on the existence of nesting wave-vectors. As shown in Fig. 4(b), while the instability in the r_{\perp} sector is related to two intra-band nesting wave-vectors \mathbf{q}_1 and \mathbf{q}_2 , the instability in the A_{\perp} sector is related to an inter-band nesting wave-vector \mathbf{q}_3 .

Since the instabilities $\chi_{z\text{-BOP}}^{r_{\perp}}$ and $\chi_{z\text{-BOP}}^{A_{\perp}}$ are nearly degenerated any small change in the model can push the instability in one channel in favor of the other, or even one can expect a mixing of both. While the instability in the sector $\chi_{z\text{-BOP}}^{r_{\perp}}$ indicates the freezing of the real part of the out-of-plane bond field r_{\perp} , the instability in the sector $\chi_{z\text{-BOP}}^{A_{\perp}}$ indicates the freezing of the imaginary part of the out-of-plane bond field A_{\perp} . In addition, the z-BOP follows a lattice pattern with ordered momentum \mathbf{q}_c . In Fig. 3(e), for simplicity, we sketched a picture of such pattern for the commensurate case $\mathbf{q}_c = (\pi, \pi)$.

In addition, the presence of a z-BOP below $T_c^{\text{z-BOP}}$ opens a gap ϕ in the system. In Appendix D we present the gap equation for ϕ , which for simplicity is considered to be real, and we assumed the incommensurate wave vector \mathbf{q}_c for each J_{\perp} [Fig. 3(d)] as the ordered momentum of the z-BOP. Then, we focus on the instability from $\chi_{z\text{-BOP}}^{r_{\perp}}$, which on the other hand is very close to the instability from $\chi_{z\text{-BOP}}^{A_{\perp}}$.

Now, we compare the solution of the gap equation for ϕ with the instability temperatures obtained from the susceptibilities. In Fig. 5(a) we present results that show that the gap equation for ϕ represents a reasonable approximation. Solid green line is the result showed in Fig. 3(b) for $T_c^{\text{z-BOP}}$ versus doping for $J_{\perp}/t = 0.8$ and $t'/t = 0.15$. Violet line is $T_c^{\text{z-BOP}}$ obtained from the instability of $\chi_{z\text{-BOP}}^{r_{\perp}}$ for a fix $\mathbf{q}_c = (\pi, 0.7\pi)$. The difference between green and violet lines occurs at temperatures

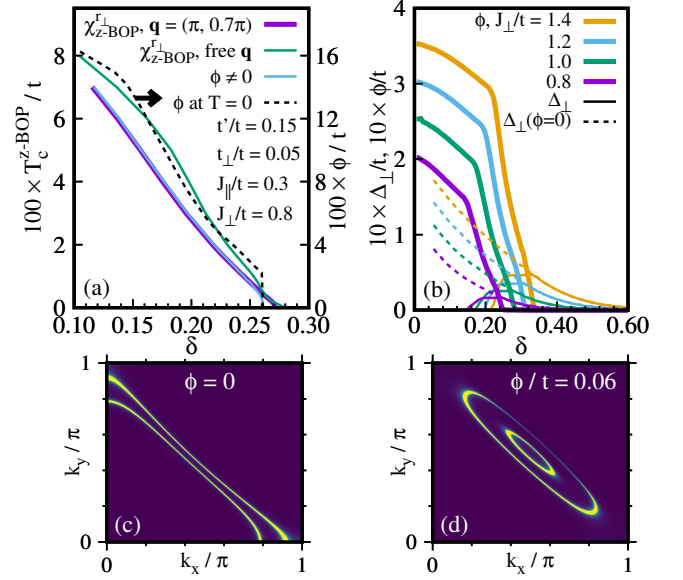


FIG. 5. (a) Green solid line shows $T_c^{\text{z-BOP}}$ versus doping. Violet solid line is the same as green solid line but searching for the instability for a fix $\mathbf{q} = (\pi, 0.7\pi)$. Blue solid line shows $T_c^{\text{z-BOP}}$ versus doping obtained when the z-BOP gap ϕ becomes nonzero. Black dashed line shows ϕ (measured on the right y -axis scale) versus doping at $T = 0$. (b) The superconducting Δ_{\perp} (thin lines) and z-BOP ϕ gaps (thick lines) versus doping for the competing case (solid lines) for $J_{\perp}/t = 0.8, 1.0, 1.2,$ and 1.4 . Dashed lines show the superconducting Δ_{\perp} versus doping without competition with the z-BOP, same as Fig. 2(a). (c) The two-sheets FS for $\delta = 0.20$ and $\phi = 0$. (d) The same as (c) for $\phi/t = 0.06$ where, for simplicity, an ordered momentum $\mathbf{q}_c = (\pi, \pi)$ was chosen.

where the ordered momentum moves from $(\pi, 0.7\pi)$ towards (π, π) [see Fig. 3(d)]. Blue solid line shows $T_c^{\text{z-BOP}}$ versus doping obtained when the z-BOP gap ϕ becomes nonzero. Thus, $T_c^{\text{z-BOP}}$ is the temperature where the z-BOP susceptibility diverges and, as should be, the z-BOP gap becomes non zero. Black dashed line shows ϕ versus doping at $T = 0$. ϕ decreases with increasing doping and goes to zero at a QCP [Fig. 3(b)].

In Fig. 5(c) we show the two-sheets Fermi surface (FS) for $\delta = 0.20$ in the normal state ($T > T_c^{\text{z-BOP}}$, i.e., $\phi = 0$). The two-sheets splitting comes from t_{\perp} and the contribution χ' [see Eq. (A9) and Eq. (A12)] to the inter-plane hopping. Figure 5(d) shows the two-sheets FS surface at $T = 0$ for $\phi/t = 0.06$. Here, for simplicity we use $\mathbf{q}_c = (\pi, \pi)$ instead of $\mathbf{q}_c = (\pi, 0.7\pi)$. Thus, inside the z-BOP, below $T_c^{\text{z-BOP}}$, the FS is formed by splitted pockets, indicating that in the z-BOP the FS is not fully gapped, and the system remains metallic with a possible pseudogap-like feature.

C. Competition between z-BOP and superconductivity

Having showed the results for the superconductivity and z-BOP separately, in the last two sections, we now look into the competition between the two. According to Fig. 2(a) T_c increases with decreasing doping. For instance, if for $\delta = 0.5$ the superconducting critical temperature is high (~ 80 K), for lower dopings possibly unrealistic high values of T_c can be expected, which is indeed hard to believe. On the other hand, in the above section we described the existence of a z-BOP instability triggered by J_\perp . Then, as in the case of the d CDW in the 2D t - J model [82], a competition between both phases, i.e., superconductivity and z-BOP, is expected.

For discussing the above picture, in Appendix E we propose a theoretical framework for studying the superconducting Δ_\perp , the z-BOP gap ϕ , and their competition [Eq. (E5) and Eq. (E6)], where we consider the incommensurate wave vector \mathbf{q}_c as the ordered momentum of the z-BOP.

Figure 5(b) shows results at $T = 0$ for $J_\perp/t = 0.8, 1.0, 1.2,$ and 1.4 , where we use the corresponding \mathbf{q}_c for each J_\perp [Fig. 3 (d)]. The superconducting gaps Δ_\perp for each case show a dome behavior with an optimal doping at $\delta \sim 0.25$ - 0.35 close to the doping where the z-BOP is developed for each J_\perp . Without competition between superconductivity and z-BOP, i.e., if $\phi = 0$ is assumed in the calculation, Δ_\perp continues increasing with decreasing doping as showed by the dashed lines. In other words, if z-BOP is removed superconductivity tends to increase with decreasing doping, as we mentioned when discussing Fig. 2(a).

A recent density matrix renormalization group study in the type II t - J model for bilayer nickelates [83] also suggests the existence of a superconducting dome with a maximum at $\delta \sim 0.4$ - 0.5 .

III. POSSIBLE IMPLICATIONS WITH THE PHENOMENOLOGY OF PRESSURIZED NICKELATES.

In this section we make a possible contact between the previous results and the phenomenology of pressurized nickelates. Considering the fact that our results are obtained on the basis of a minimal model in a given approximation, and from the experimental side it is not clear what is the value of J_\perp and how it changes with doping and pressure, our discussions should be considered qualitatively.

For $\delta = 0.50$, $J_\perp/t = 1.4$, and $t'/t = 0.15$ [43] we obtain a superconducting critical temperature $T_c/t \sim 0.007$ [Fig. 2(b)], which corresponds to $T_c \sim 80$ K, i.e., of the same order of that reported in bilayer nickelates [1]. For this estimate we have assumed a band width of $t/2 = 0.5$ eV [43, 84].

If we assume that the increase of pressure induces an

increase of J_\perp , the result of Fig. 2(c) offers a possible explanation for the observation that T_c increases with pressure. In addition, superconductivity is expected only if J_\perp is larger than a certain value which, for instance, is $J_\perp/t \sim 0.9$ for $t'/t = 0.15$ at $\delta = 0.5$. This feature might explain the presence of a critical pressure (i.e., a critical J_\perp) for the appearance of superconductivity, as observed in experiments.

Interestingly, if J_\perp is vanishingly small only in-plane d -wave superconductivity is possible below $\delta \lesssim 0.30$ [inset of Fig. 2(a)], similar to cuprates where $J_\perp = 0$. It can be shown that for $\delta = 0.16$, which corresponds approximately to optimally doping, the superconducting critical temperature is about $T_c/t \sim 0.007$, i.e., $T_c \sim 80$ K which is similar to that observed in cuprates [54]. However, if $J_\perp > J_\parallel$, as discussed for nickelates [35], our theory predicts that J_\perp disfavors in-plane d -wave superconductivity for all dopings [see Fig. 2(a)].

To our knowledge there are no reports yet of underdoped and/or overdoped nickelates under pressure. But certainly, it is expected and desirable that these experiments come in the near future, and they are important for the understanding of the phenomenology of these materials. If at quarter filling (i.e., $\delta = 0.5$) we already find $T_c \sim 80$ K and pressurized nickelates are correlated systems, we can expect larger values for T_c at lower doping. In fact, this is a key feature in the 2D t - J model in the context of cuprates. The lower the doping is, the less diluted are the charge carriers and J is more effective for pairing. According to Fig. 2(a) T_c increases monotonically with decreasing doping, reaching possibly unrealistic high values of T_c . One possible expectation is that at lower dopings some instability to a new phase develops, competes with superconductivity, and pushes down T_c as in cuprates. Beyond mean-field level we have obtained a z-BOP which can compete with superconductivity, leading to a dome in T_c as a function of doping, as shown in Fig. 5(b). The dome presented in Fig. 5(b) has optimal dopings at $\delta \sim 0.25$ - 0.35 depending on the value of J_\perp . Of course this analysis must be taken with caution because it assumes that the system can be doped at a fixed pressure keeping J_\perp rather constant, which is in fact unknown and nontrivial.

Since the z-BOP is basically a charge instability it would be interesting to search for that using X-ray techniques, as those used for studying the charge order in cuprates superconductors [54]. On the other hand z-BOP and/or its fluctuations can get coupled with the lattice and phonons. In addition, it would be also interesting to see if the z-BOP is obtained by using other theoretical methods. For instance, we believe that the slave-boson approach beyond mean-field would have to show the z-BOP, as it shows different bond order phases triggered by J_\parallel in the 2D t - J model [77]. However, in the present model we expect the z-BOP to be stronger because $J_\perp > J_\parallel$.

At this point it is important to remark that although the value of J_\perp is unknown, some reports estimate $J_\perp \gtrsim$

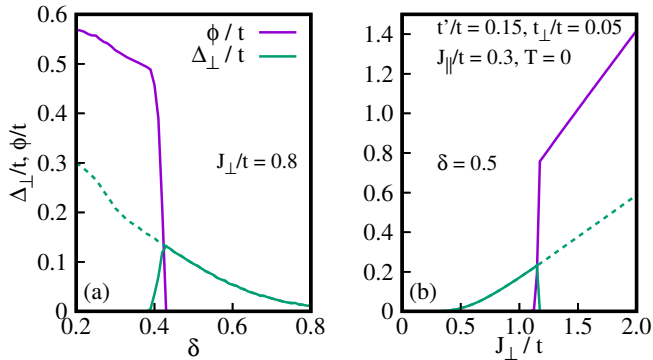


FIG. 6. (a) The superconducting Δ_{\perp} and z-BOP ϕ gaps versus doping for the competing case (solid lines). Dashed line shows the superconducting Δ_{\perp} versus doping without competition with the z-BOP. (b) Δ_{\perp} and ϕ as a function of J_{\perp} . Dashed line is the result for Δ_{\perp} without the coupling between superconductivity and z-BOP, while for solid lines both phases compete. See text for discussions.

$2J_{\parallel}$ [36]. This means that a value of $J_{\perp}/t = 1.4$ may be too large. However, we wish to emphasize once more the qualitative aspect of our results which are obtained on a basis of a minimal model in a given approximation. For instance, if we chose the prefactor $3J_{\perp}/4$ and $3J_{\perp}/2$ on the right hand side of equations Eq. (E5) and Eq. (E6), respectively, instead of $J_{\perp}/4$ and $J_{\perp}/2$, we obtain the result of Fig. 6(a) for $J_{\perp}/t = 0.8$; a value closer to the one reported in Ref. 36. In this case we obtain a dome in T_c with maximum at $\delta \sim 0.45$, closer to $\delta = 0.5$.

Some reports in pressurized nickelates discuss the existence of a strange metal phase at high temperatures [1, 11, 85]. Then, it will be very interesting to perform experiments as a function of doping and see if a dome in T_c is observed, which may indicate the presence of a pseudogap, and a strange metal phase at high temperatures around optimal doping as in cuprates, and in addition a Fermi liquid phase at low temperatures and high doping. Whether a possible pseudogap can be associated with z-BOP is not straightforward, but it is suggestive that, as in the 2D t - J model [82], a bond-order instability might compete with superconductivity and leads to a dome behavior for T_c .

In Ref. [51] a dome of T_c as a function of pressure was reported, i.e., T_c increases with pressure reaching the maximum at 18 GPa, and for larger pressures T_c is suppressed. If the increasing of pressure means *crudely* an increase of J_{\perp} , then Fig. 6(b) could offer a possible explanation: Superconductivity increases until $J_{\perp}/t \sim 1.1$ where the z-BOP develops, leading to a decrease of Δ_{\perp} for larger J_{\perp} (pressure). Although in the experiment the decrease of T_c with pressure is smoother, our approximation shows the main picture.

IV. DISCUSSIONS AND CONCLUSION

Inspired by the high value of the superconducting critical temperature T_c [1] in pressurized nickelates and the similarities with high- T_c cuprate superconductors [50], we assumed that pressurized bilayer nickelates are strongly correlated systems, and studied the consequences of such assumption. Since recent experiments indicate that pressurized nickelates are really bulk high- T_c superconductors, a kind of t - J model can be expected to describe the physics of these materials. In this context, the t - J_{\parallel} - J_{\perp} can be considered as a minimal model [35, 36]. We studied this model in a large- N approximation based on the path integral representation for Hubbard operators. The model contains tendencies to in-plane d -wave superconductivity triggered by J_{\parallel} , out-of-plane s -wave superconductivity due to J_{\perp} , and the competition of both. Since superconductivity in nickelates occurs at quarter filling, which is a high hole doping value ($\delta = 0.5$) for the 2D t - J model for cuprates, the presence of J_{\perp} becomes relevant.

It is well known that the large- N approximation overestimates charge over magnetic excitations [74]. Since the $d_{x^2-y^2}$ orbital in nickelates is quarter filling, this large hole doping ($\delta = 0.5$) and the fact that it seems that pressurized nickelates are far from a magnetic order [16, 17] suggest that the large- N approach is a good approximation for describing the pressurized nickelates.

J_{\perp} can easily lead to an s -wave out-of-plane superconductivity at $\delta = 0.5$ with high T_c values as in the experiments [Figs. 2(a)-(b)]. In addition, we found that a lower limit for J_{\perp} exists in order to get superconductivity [Fig. 2(c)]. If J_{\perp} is smaller than this lower limit, superconductivity is not expected at quarter filling, which can be associated to the fact that the increasing of pressure increases J_{\perp} and superconductivity emerges.

At mean-field level we obtain that T_c increases steeply with decreasing doping, reaching possible unrealistic values for T_c at low doping. However, beyond mean-field level we obtain an instability to an out-of-plane bond-order phase z-BOP below a critical temperature $T_c^{\text{z-BOP}}$ with an incommensurate ordered momentum $\mathbf{q}_c = (1, q)\pi$ at $T = 0$. $T_c^{\text{z-BOP}} = 0$ at a QCP close to $\delta \sim 0.25$ - 0.40 , depending on the values of J_{\perp} and t' [Fig. 3(a)]. The competition of z-BOP (and also possibly with its fluctuations) and superconductivity leads to a dome behavior of T_c [Figs. 5(b) and 6(a)]. This suggests the possible presence of a pseudogap in pressurized nickelates, similar to cuprates. This fact may be consistent with the strange metal behavior at high temperature discussed in some reports [1, 11, 85]. Then, it is worthwhile to study the behavior of T_c as a function of doping.

If the increase of pressure increases J_{\perp} it may explain *qualitatively* the dome shape behavior for superconductivity as a function of pressure observed experimentally [51]. With increasing pressure, superconductivity develops at a certain value of pressure, where the minimum value of J_{\perp} for triggering superconductivity is reached.

With increasing pressure even more, T_c increases until a value of pressure (J_\perp) where the z -BOP develops and T_c goes down with a further pressure increase [Fig. 6(b)].

Finally, we like to emphasize that our results should be considered at a qualitative level and, in spite of the limitations of our approach, we have obtained some positive results arising from this first view of the problem. This motivates future calculations in the framework of the full approach (Appendix A), which of course is a big challenge. One important and nontrivial issue is about the role of the out-of-plane Coulomb interaction V_\perp . If the increase of pressure increases J_\perp , an increase of V_\perp is also expected, as suggested in the context of organic materials [60], and superconductivity can be negligible at mean-field level if $V_\perp \sim J_\perp$. Preliminary calculations beyond mean-field suggest, as in Ref. [70] for the 2D t - J model, that the main role of the dressed D_{ab} [Eq. (A25)] on superconductivity is to screen out V_\perp due to the fluctuations of $\delta\lambda_\alpha$ [Eq. (A14)] which enforce the nodouble occupancy constraint.

ACKNOWLEDGMENTS

The authors thank to M. Hepting, H. Yamase, and L. Zinni for illuminating discussions. A part of the results presented in this work was obtained by using the facilities of the CCT-Rosario Computational Center, member of the High Performance Computing National System (SNCAD, Mincyt- Argentina). A. Greco acknowledges the Max-Planck-Institute for Solid State Research in Stuttgart for hospitality and financial support.

Appendix A: Large- N expansion based on the path integral for Hubbard operators. Extension to the bilayer t - J_\parallel - J_\perp

It is nontrivial to study the t - J model because of the local constraint that prohibit double occupancy at any site. In addition, the operators involved in the t - J model are Hubbard operators \hat{X} [68], which satisfy nonstandard commutation rules. In the language of Hubbard operators $\tilde{c}_{i\sigma}^\dagger = \hat{X}_i^{\sigma 0}$, $\tilde{c}_{i\sigma} = \hat{X}_i^{0\sigma}$, $S_i^+ = \hat{X}_i^{\uparrow\downarrow}$, $S_i^- = \hat{X}_i^{\downarrow\uparrow}$, $n_i = \hat{X}_i^{\uparrow\uparrow} + \hat{X}_i^{\downarrow\downarrow}$, and \hat{X}_i^{00} describes the number of doped holes; the z component of the spin operator is described by $S_i^z = \frac{1}{2}(\hat{X}_i^{\uparrow\uparrow} - \hat{X}_i^{\downarrow\downarrow})$. The operators $\hat{X}_i^{\sigma 0}$ and $\hat{X}_i^{0\sigma}$ are called fermionlike, whereas the operators $\hat{X}_i^{\sigma\sigma'}$ and \hat{X}_i^{00} are bosonlike. We employ a large- N technique based on the path integral representation for Hubbard operators for the 2D t - J model in the context of cuprates [67, 74]. In the large- N approach the number of spin components is extended from 2 to N and the physical quantities are computed in powers of $1/N$. One of the advantages of this method is that it treats all possible charge excitations on an equal footing [74]. There are two major difficulties in the Hamiltonian Eq. (1): the complicated commutation rules of the Hubbard operators [68] and the absence

of a small parameter. A popular method to handle the former difficulty is to use slave particles. For instance, in the slave-boson method [86] the original fermionlike $\hat{X}^{0\sigma}$ operator is written as a product of usual bosonic (holons) and fermionic (spinons) operators. This scheme introduces a gauge field, which requires a gauge fixing and the introduction of a Faddeev-Popov determinant [87]. Gauge fluctuations should be taken into account beyond mean-field theory and the slave particles need to be convoluted to form the original fermionic operator \tilde{c} . Since our method work on the basis of path integral for Hubbard operators our fermions are just related to the Hubbard operators and not with the spinons of the slave-boson technique, and we do not have to deal with the Bose condensation of holons.

If $t_\perp = J_\perp = 0$ the Hamiltonian Eq. (1) reduces to two 2D decoupled t - J models which were treated in [67]. See also the Appendix of Ref. [88] for a more detailed formulation of the path integral representation for Hubbard operators and the large- N approach.

For clarifying ideas, here we focus on the case of finite t_\perp and J_\perp , which on the other hand are the new and relevant contributions of interest for discussing pressurized nickelates.

In terms of Hubbard operators the last two terms of Eq. (1) can be written as

$$t_\perp \sum_{i,\sigma,\alpha} \hat{X}_{i,\alpha}^{\sigma 0} \hat{X}_{i,\bar{\alpha}}^{0\sigma} + \frac{J_\perp}{4} \sum_{i,\sigma,\sigma',\alpha} (\hat{X}_{i,\alpha}^{\sigma\sigma'} \hat{X}_{i,\bar{\alpha}}^{\sigma'\sigma} - \hat{X}_{i,\alpha}^{\sigma\sigma} \hat{X}_{i,\bar{\alpha}}^{\sigma'\sigma'}) \quad (\text{A1})$$

where $\alpha = 1, 2$ is an index that identifies each plane.

Following [67, 88] we write

$$\hat{X}_{i,\alpha}^{\sigma\sigma'} = \frac{\hat{X}_{i,\alpha}^{\sigma 0} \hat{X}_{i,\alpha}^{0\sigma'}}{\hat{X}_{i,\alpha}^{00}} \quad (\text{A2})$$

We extend the spin projections from $\sigma = \uparrow, \downarrow$ to $p = 1, \dots, N$, rescale the Hamiltonian parameters to t_\perp/N , J_\perp/N , and write the fermionlike fields as follows:

$$f_{ip,\alpha}^\dagger = \frac{1}{\sqrt{N\delta/2}} \hat{X}_{i,\alpha}^{p0}, \quad (\text{A3})$$

$$f_{ip,\alpha} = \frac{1}{\sqrt{N\delta/2}} \hat{X}_{i,\alpha}^{0p}. \quad (\text{A4})$$

where δ is the hole doping rate away from half-filling. The fermion variable $f_{ip,\alpha}$ is proportional to $\hat{X}_{i,\alpha}^{0p}$ and should not be associated with the so-called spinon in the slave-boson method.

The operator $\hat{X}_{i,\alpha}^{00}$ is written in terms of the fluctuations of the number of holes $\delta R_{i,\alpha}$ as

$$\hat{X}_{i,\alpha}^{00} = N \frac{\delta}{2} (1 + \delta R_{i,\alpha}). \quad (\text{A5})$$

Making these changes the exchange interaction term (J_\perp -term) contains four fermion fields and the two bosons

in the denominator. They can be decoupled through a Hubbard-Stratonovich transformation by introducing the field Δ'_i ,

$$\Delta'_i = \frac{J_\perp}{4N} \sum_p \frac{f_{ip,1}^\dagger f_{ip,2}}{\sqrt{(1 + \delta R_{i,1})(1 + \delta R_{i,2})}}. \quad (\text{A6})$$

This field describes out-of-plane bond-charge fluctuations.

Therefore, Eq. (A1) is written as

$$\begin{aligned} & t_\perp \frac{\delta}{2} \sum_{i,p,\alpha} f_{ip,\alpha}^\dagger f_{ip,\bar{\alpha}} + \frac{2N}{J_\perp} \sum_i \Delta_i^\dagger \Delta'_i \\ & - \sum_{i,p} \left(\frac{f_{ip,1}^\dagger f_{ip,2}}{\sqrt{(1 + \delta R_{i,1})(1 + \delta R_{i,2})}} \Delta'_i + h.c. \right) \end{aligned} \quad (\text{A7})$$

The out-of-plane bond field Δ'_i is parameterized as

$$\Delta'_i = \chi' (1 + r_{\perp,i} + iA_{\perp,i}), \quad (\text{A8})$$

where $r_{\perp,i}$ and $A_{\perp,i}$ correspond to the real and imaginary parts of the out-of-plane bond-field fluctuations, respectively, and χ' is a static mean-field value. Finally, we expand the term $1/\sqrt{1 + \delta R}$ in powers of δR , which generates various interactions between fermions and bosons. The number of the interactions considered in the theory is controlled in powers of $1/N$.

Putting together the above terms for the out-of-plane Hamiltonian Eq. (A1) and the in-plane terms [67, 88], the effective theory for Eq. (1) is described in terms of fermions, bosons, and their interactions.

In terms of the spinor $(f_{\mathbf{k}p,1}, f_{\mathbf{k}p,2})$ we define a 2×2 electron Green function which is $O(1)$

$$G_{\alpha\beta}^{(0)}(\mathbf{k}, i\nu_n) = \begin{pmatrix} i\nu_n - \varepsilon_{\mathbf{k}}^\parallel & -(t_\perp \delta/2 - \chi') \\ -(t_\perp \delta/2 - \chi') & i\nu_n - \varepsilon_{\mathbf{k}}^\parallel \end{pmatrix}^{-1}, \quad (\text{A9})$$

with

$$\begin{aligned} \varepsilon_{\mathbf{k}}^\parallel &= -2 \left(t \frac{\delta}{2} + \chi \right) (\cos k_x + \cos k_y) \\ &+ 4t' \frac{\delta}{2} \cos k_x \cos k_y - \mu, \end{aligned} \quad (\text{A10})$$

For a given doping δ , the chemical potential μ , χ , and χ' are determined self-consistently by solving

$$\chi = \frac{J_\parallel}{4N_s} \sum_{\mathbf{k}, i\nu_n} (\cos k_x + \cos k_y) G_{11}^{(0)}(\mathbf{k}, i\nu_n), \quad (\text{A11})$$

$$\chi' = \frac{J_\perp}{2N_s} \sum_{\mathbf{k}, i\nu_n} G_{12}^{(0)}(\mathbf{k}, i\nu_n), \quad (\text{A12})$$

and

$$1 - \delta = \frac{2}{N_s} \sum_{\mathbf{k}, i\nu_n} G_{11}^{(0)}(\mathbf{k}, i\nu_n), \quad (\text{A13})$$

In the above expressions N_s and ν_n are the number of sites in each plane and a fermionic Matsubara frequency, respectively. $G_{12}^{(0)}$ and $G_{11}^{(0)}$ are the elements (1, 2) and (1, 1) of the Green function, respectively.

In the context of the t - J_\parallel - J_\perp model using a path-integral representation for Hubbard operators a 14-component bosonic field is defined as:

$$\begin{aligned} \delta X^a &= (\delta R_1, \delta \lambda_1, \delta R_2, \delta \lambda_2, r_1^x, r_1^y, A_1^x, A_1^y, \\ & r_2^x, r_2^y, A_2^x, A_2^y, r_\perp, A_\perp), \end{aligned} \quad (\text{A14})$$

where δR_α describes fluctuations of the number of holes at a given site (the site index is excluded for clarity) in the plane α and it is related to on-site charge fluctuations in each plane, $\delta \lambda_\alpha$ is the fluctuation of the Lagrange multiplier introduced to enforce the constraint that prohibits the double occupancy at any site in each plane, and r_α^x and r_α^y (A_α^x and A_α^y) describe fluctuations of the real (imaginary) part of the in-plane bond field coming from the J_\parallel -term. r_\perp and A_\perp are the fluctuations of the real and imaginary part, respectively, of the out-of-plane bond field coming from the J_\perp -term.

Following [67, 74] we obtain

$$[D_{ab}^{(0)}(\mathbf{q}, i\omega_n)]^{-1} = N \begin{pmatrix} D_A^{(0)} & D_B^{(0)} & 0 & 0 & 0 \\ D_B^{(0)} & D_A^{(0)} & 0 & 0 & 0 \\ 0 & 0 & D_C^{(0)} & 0 & 0 \\ 0 & 0 & 0 & D_C^{(0)} & 0 \\ 0 & 0 & 0 & 0 & D_D^{(0)} \end{pmatrix}, \quad (\text{A15})$$

a 14×14 bare bosonic propagator $D_{ab}^{(0)}(\mathbf{q}, i\omega_n)$ associated with δX^a , where ω_n is a bosonic Matsubara frequency. The matrices $D_{A-D}^{(0)}$ are

$$D_A^{(0)} = \begin{pmatrix} -\frac{\delta^2}{2} J(\mathbf{q}) & \frac{\delta}{2} \\ \frac{\delta}{2} & 0 \end{pmatrix} \quad (\text{A16})$$

$$D_B^{(0)} = \begin{pmatrix} -\frac{\delta^2}{2} J_\perp/2 & 0 \\ 0 & 0 \end{pmatrix} \quad (\text{A17})$$

$$D_C^{(0)} = \begin{pmatrix} \frac{4\chi^2}{J_\parallel} & 0 & 0 & 0 \\ 0 & \frac{4\chi^2}{J_\parallel} & 0 & 0 \\ 0 & 0 & \frac{4\chi^2}{J_\parallel} & 0 \\ 0 & 0 & 0 & \frac{4\chi^2}{J_\parallel} \end{pmatrix} \quad (\text{A18})$$

$$D_D^{(0)} = \begin{pmatrix} \frac{4\chi'^2}{J_\perp} & 0 \\ 0 & \frac{4\chi'^2}{J_\perp} \end{pmatrix}, \quad (\text{A19})$$

where $J(\mathbf{q}) = (J_\parallel/2)(\cos q_x + \cos q_y)$. Note that $D_{ab}^{(0)}$ is $O(1/N)$.

The theory gives also three- and four-legs vertices. The three-legs vertex $\Lambda_{\alpha\beta,a}$ represents the interaction of a

fermion from the plane α that ends at plane β after interacting with a boson δX^a . The nonzero components of this vertex are

$$\begin{aligned} \Lambda_{\alpha\alpha,a}(\mathbf{k}, \mathbf{q}) = & - \left[\frac{i\nu_n + i\nu'_n}{2} + \mu + 2\chi \sum_{\eta=x,y} \cos\left(k_\eta - \frac{q_\eta}{2}\right) \cos \frac{q_\eta}{2}, 1, \right. \\ & - 2\chi \cos\left(k_x - \frac{q_x}{2}\right), -2\chi \cos\left(k_y - \frac{q_y}{2}\right), \\ & \left. 2\chi \sin\left(k_x - \frac{q_x}{2}\right), 2\chi \sin\left(k_y - \frac{q_y}{2}\right) \right] \end{aligned} \quad (\text{A20})$$

for each component $a = \delta R_\alpha, \delta\lambda_\alpha, r_\alpha^x, r_\alpha^y, A_\alpha^x, A_\alpha^y$, and

$$\begin{aligned} \Lambda_{12,a}(\mathbf{k}, \mathbf{q}) = & - \left(\frac{\chi'}{2}, \frac{\chi'}{2}, -\chi', -i\chi' \right) \\ \Lambda_{21,a}(\mathbf{k}, \mathbf{q}) = & - \left(\frac{\chi'}{2}, \frac{\chi'}{2}, -\chi', i\chi' \right) \end{aligned} \quad (\text{A21})$$

for each component $a = \delta R_1, \delta R_2, r_\perp, A_\perp$.

The four-legs vertex $\Lambda_{\alpha\beta,ab}$ represents a fermion from the plane α that ends at plane β after interacting with the bosons δX^a and δX^b . The nonzero components of this vertex are

$$\Lambda_{\alpha\alpha,ab} = \begin{bmatrix} F_{\mathbf{q}} & 1/2 \\ 1/2 & 0 \end{bmatrix} \quad (\text{A22})$$

for component $a, b = \delta R_\alpha, \delta\lambda_\alpha$, where

$$\begin{aligned} F_{\mathbf{q}} = & \frac{i\nu_n + i\nu'_n}{2} + \mu + \chi \sum_{\eta=x,y} \cos\left(k_\eta + \frac{q_\eta + q'_\eta}{2}\right) \\ & \times \left[\cos\left(\frac{q_\eta + q'_\eta}{2}\right) + \cos \frac{q_\eta}{2} \cos \frac{q'_\eta}{2} \right], \end{aligned}$$

$$\begin{aligned} \Lambda_{\alpha\alpha,ab} = & -\chi \left[\cos\left(k_x - \frac{q_x + q'_x}{2}\right), \cos\left(k_y - \frac{q_y + q'_y}{2}\right), \right. \\ & \left. -\sin\left(k_x - \frac{q_x + q'_x}{2}\right), -\sin\left(k_y - \frac{q_y + q'_y}{2}\right) \right] \end{aligned} \quad (\text{A23})$$

for component $a = \delta R_\alpha$, and $b = r_\alpha^x, r_\alpha^y, A_\alpha^x$, and A_α^y , and

$$\Lambda_{12,ab} = -\frac{\chi'}{4} \begin{bmatrix} -3/2 & -1/2 & 1 & i \\ -1/2 & -3/2 & 1 & i \\ 1 & 1 & 0 & 0 \\ i & i & 0 & 0 \end{bmatrix} \quad (\text{A24})$$

for component $a, b = \delta R_1, \delta R_2, r_\perp, A_\perp$. For the vertices $\Lambda_{21,ab}$ the components involving A_\perp change sign [right column and bottom row of Eq. (A24)]. Note that the vertices are $O(1)$.

Using the propagators [Fig. 7(a)] and vertices [Fig. 7(b)] we can compute the bosonic self energy $\Pi_{ab}(\mathbf{q}, i\omega_n)$

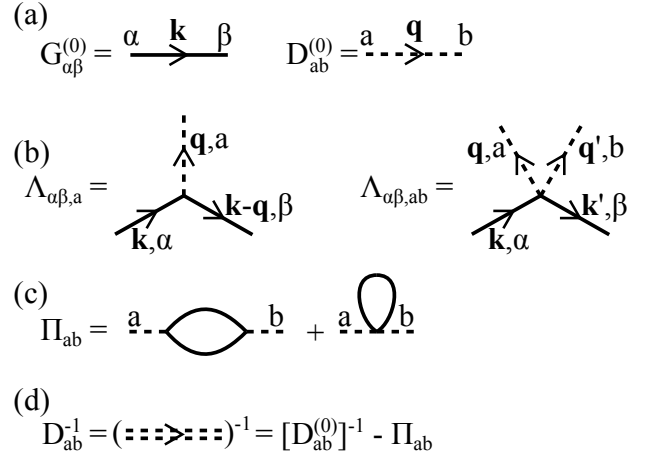


FIG. 7. (a) Bare fermionic $G_{\alpha\beta}^{(0)}$ and bosonic $D_{ab}^{(0)}$ propagators, solid and dashed lines, respectively. (b) $\Lambda_{\alpha\beta,a}$ and $\Lambda_{\alpha\beta,ab}$ are the three- and four-legs vertices, respectively. (c) Π_{ab} is the bosonic self energy. (d) Double dashed line is the dressed bosonic propagator D_{ab} beyond mean-field level.

[Fig. 7(c)] which is used in the Dyson equation to compute the dressed bosonic propagator $D_{ab}(\mathbf{q}, i\omega_n)$ [Fig. 7(d)],

$$D_{ab}^{-1}(\mathbf{q}, i\omega_n) = \left[D_{ab}^{(0)}(\mathbf{q}, i\omega_n) \right]^{-1} - \Pi_{ab}(\mathbf{q}, i\omega_n). \quad (\text{A25})$$

The order in $1/N$ of any calculated quantity is estimated by counting the number of propagators and vertices involved in the calculation [67].

Appendix B: The exchange J_\perp subspace

As discussed in the main text, the relevant and new quantity is the out-of-plane exchange J_\perp . Then here it is useful and instructive to focus on this sector, which is defined by the subspace generated by the elements 13 and 14 of the δX^a [Eq. (A14)], i.e., r_\perp and A_\perp .

In this subspace we have the following bare bosonic propagator and vertices:

a) The 2×2 bare bosonic propagator

$$[D_{z\text{-BOP}}^{(0)}(\mathbf{q}, i\omega_n)]^{-1} = N \begin{pmatrix} \frac{4\chi'^2}{J_\perp} & 0 \\ 0 & \frac{4\chi'^2}{J_\perp} \end{pmatrix} \quad (\text{B1})$$

associated to the out-of-plane bond-field fluctuations r_\perp and A_\perp .

b) The three-legs vertices

$$\begin{aligned} \Lambda_{12,a} &= (\chi', i\chi') \\ \Lambda_{21,a} &= (\chi', -i\chi') \end{aligned} \quad (\text{B2})$$

for $a = r_\perp, A_\perp$.

The 2×2 z-BOP bosonic self-energy is the sector 13-14 of Π_{ab} ,

$$\Pi_{ab}(\mathbf{q}, i\omega_n) = \sum_{k, \alpha, \beta} \Lambda_{\alpha\bar{\alpha}, a} G_{\alpha\beta}^{(0)}(k) G_{\bar{\alpha}\bar{\beta}}^{(0)}(k-q) \Lambda_{\beta\bar{\beta}, b}. \quad (\text{B3})$$

where $a, b = 13, 14$. Here we use the simplified notation q meaning \mathbf{q} , $i\omega_n$, k meaning \mathbf{k} , $i\nu_n$, and $k-q$ meaning $\mathbf{k}-\mathbf{q}$, $i\nu_n - i\omega_n$. Using Eq. (B2) for the vertices we can explicitly write four contributions

$$\begin{aligned} \Pi_{ab}(\mathbf{q}, i\omega_n) = \sum_k (\chi')^2 & \left[\begin{pmatrix} 1 & i \\ i & -1 \end{pmatrix} G_{11}^{(0)}(k) G_{22}^{(0)}(k-q) + \right. \\ & \begin{pmatrix} 1 & -i \\ i & 1 \end{pmatrix} G_{12}^{(0)}(k) G_{21}^{(0)}(k-q) + \\ & \begin{pmatrix} 1 & i \\ -i & 1 \end{pmatrix} G_{21}^{(0)}(k) G_{12}^{(0)}(k-q) + \\ & \left. \begin{pmatrix} 1 & -i \\ -i & -1 \end{pmatrix} G_{22}^{(0)}(k) G_{11}^{(0)}(k-q) \right]. \end{aligned} \quad (\text{B4})$$

From the inverse of Eq. (A9) we can see that $G_{11}^{(0)} = G_{22}^{(0)}$, and $G_{12}^{(0)} = G_{21}^{(0)}$. Using this we can write Eq. (B4) as

$$\begin{aligned} \Pi_{ab}(\mathbf{q}, i\omega_n) = \sum_k (\chi')^2 & \left[\begin{pmatrix} 2 & 0 \\ 0 & -2 \end{pmatrix} G_{11}^{(0)}(k) G_{11}^{(0)}(k-q) + \right. \\ & \left. \begin{pmatrix} 2 & 0 \\ 0 & 2 \end{pmatrix} G_{12}^{(0)}(k) G_{12}^{(0)}(k-q) \right], \end{aligned} \quad (\text{B5})$$

where it can be seen that the elements $\Pi_{1314} = \Pi_{1413} = 0$, and the explicit expressions for Π_{1313} and Π_{1414} are

$$\Pi_{1313} = -(\chi')^2 \sum_{\mathbf{k}} (g^{--} + g^{++}) \quad (\text{B6})$$

$$\Pi_{1414} = -(\chi')^2 \sum_{\mathbf{k}} (g^{+-} + g^{-+}), \quad (\text{B7})$$

where

$$\begin{aligned} g^{\alpha\beta} &= \frac{n_F(\varepsilon_{\mathbf{k}-\mathbf{q}}^\alpha) - n_F(\varepsilon_{\mathbf{k}}^\beta)}{i\omega_n + \varepsilon_{\mathbf{k}-\mathbf{q}}^\alpha - \varepsilon_{\mathbf{k}}^\beta}, \\ \varepsilon_{\mathbf{k}}^\pm &= \varepsilon_{\mathbf{k}}^\parallel \pm (t_\perp \delta/2 - \chi'), \end{aligned} \quad (\text{B8})$$

and n_F is the Fermi factor.

Then, in the J_\perp subsector the Dyson equation reads as:

$$\begin{aligned} D_{\text{z-BOP}}^{-1}(\mathbf{q}, i\omega_n) = \\ N \begin{pmatrix} \frac{4\chi'^2}{J_\perp} - \Pi_{1313}(\mathbf{q}, i\omega_n) & 0 \\ 0 & \frac{4\chi'^2}{J_\perp} - \Pi_{1414}(\mathbf{q}, i\omega_n) \end{pmatrix}, \end{aligned} \quad (\text{B9})$$

which defines the 2×2 dressed bosonic propagator beyond mean-field level [Eq. (B1)]. Thus, the renormalized $D_{\text{z-BOP}}^{-1}$ results diagonal.

Appendix C: Superconducting gap equations

For the calculation of the superconducting in-plane (Δ_\parallel) and out-of-plane (Δ_\perp) gap we introduce the four-component Nambu spinor

$$\psi_{\mathbf{k}}^\dagger = (f_{\mathbf{k}\uparrow,1}^\dagger, f_{\mathbf{k}\uparrow,2}^\dagger, f_{-\mathbf{k}\downarrow,1}, f_{-\mathbf{k}\downarrow,2}), \quad (\text{C1})$$

and the inverse of the 4×4 Nambu Green function can be written as

$$G^{-1}(\mathbf{k}, i\nu_n) = \begin{pmatrix} i\nu_n - \varepsilon_{\mathbf{k}}^\parallel & -\varepsilon_\perp & -\Delta_\parallel(\mathbf{k}) & -\Delta_\perp(\mathbf{k}) \\ -\varepsilon_\perp & i\nu_n - \varepsilon_{\mathbf{k}}^\parallel & -\Delta_\perp(\mathbf{k}) & -\Delta_\parallel(\mathbf{k}) \\ -\Delta_\parallel(\mathbf{k}) & -\Delta_\perp(\mathbf{k}) & i\nu_n + \varepsilon_{\mathbf{k}}^\parallel & \varepsilon_\perp \\ -\Delta_\perp(\mathbf{k}) & -\Delta_\parallel(\mathbf{k}) & \varepsilon_\perp & i\nu_n + \varepsilon_{\mathbf{k}}^\parallel \end{pmatrix}, \quad (\text{C2})$$

where $\varepsilon_\perp = (t_\perp \delta/2 - \chi')$, $\Delta_\parallel(\mathbf{k}) = \Delta_\parallel \gamma_d(\mathbf{k})$ and $\Delta_\perp(\mathbf{k}) = \Delta_\perp$, $i\nu_n$ is a fermionic Matsubara frequency, and $\varepsilon_{\mathbf{k}}^\parallel$ is the band dispersion in the plane [Eq. (A10)].

Then, the gap equations for Δ_\parallel and Δ_\perp are

$$\Delta_\parallel = -J_\parallel \sum_{\mathbf{k}, i\nu_n} \gamma_d(\mathbf{k}) G_{13}(\mathbf{k}, i\nu_n) \quad (\text{C3})$$

and

$$\Delta_\perp = -\frac{J_\perp}{4} \sum_{\mathbf{k}, i\nu_n} G_{14}(\mathbf{k}, i\nu_n), \quad (\text{C4})$$

and must be solved self consistently. In Eq. (C3) $\gamma_d(\mathbf{k}) = \frac{1}{2}(\cos k_x - \cos k_y)$.

Appendix D: z-BOP susceptibilities and gap equation for the z-BOP gap

The z-BOP susceptibilities are defined projecting $D_{\text{z-BOP}}$ on the eigenvectors (1, 0) and (0, 1), and are given respectively by

$$\chi_{\text{z-BOP}}^{r_\perp}(\mathbf{q}, i\omega_n) = \left[\frac{4\chi'^2}{J_\perp} - \Pi_{1313}(\mathbf{q}, i\omega_n) \right]^{-1}, \quad (\text{D1})$$

$$\chi_{\text{z-BOP}}^{A_\perp}(\mathbf{q}, i\omega_n) = \left[\frac{4\chi'^2}{J_\perp} - \Pi_{1414}(\mathbf{q}, i\omega_n) \right]^{-1}. \quad (\text{D2})$$

For the calculation of the z-BOP gap ϕ we introduce the four-component Nambu spinor

$$\psi_{\mathbf{k}}^\dagger = (f_{\mathbf{k}\sigma,1}^\dagger, f_{\mathbf{k}\sigma,2}^\dagger, f_{\mathbf{k}+\mathbf{q}_c,\sigma,1}^\dagger, f_{\mathbf{k}+\mathbf{q}_c,\sigma,2}^\dagger), \quad (\text{D3})$$

and the inverse of the 4×4 Nambu Green function for

each spin can be written as

$$G^{-1}(\mathbf{k}, i\nu_n) = \begin{pmatrix} i\nu_n - \varepsilon_{\mathbf{k}}^{\parallel} & -\varepsilon_{\perp} & 0 & -\phi \\ -\varepsilon_{\perp} & i\nu_n - \varepsilon_{\mathbf{k}}^{\parallel} & -\phi & 0 \\ 0 & -\phi & i\nu_n - \varepsilon_{\mathbf{k}+\mathbf{q}_c}^{\parallel} & -\varepsilon_{\perp} \\ -\phi & 0 & -\varepsilon_{\perp} & i\nu_n - \varepsilon_{\mathbf{k}+\mathbf{q}_c}^{\parallel} \end{pmatrix}, \quad (\text{D4})$$

where \mathbf{q}_c is the ordered momentum of the z-BOP.

Then, the gap equation for ϕ is

$$\phi = -\frac{J_{\perp}}{2} \sum_{\mathbf{k}, i\nu_n} G_{14}(\mathbf{k}, i\nu_n). \quad (\text{D5})$$

Note that Eq. (D4) is valid for a commensurated momentum such as $\mathbf{q}_c = (\pi, \pi)$. For an incommensurated momentum one should use a bigger matrix with the additional symmetry related momenta. As the values we used for \mathbf{q}_c are close to (π, π) and the $T_c^{\text{z-BOP}}$ versus doping obtained when the z-BOP gap ϕ becomes nonzero is in good agreement with the one obtained from the susceptibilities [see Fig. 5(a)], we think that using Eq. (D4) with an incommensurated momentum \mathbf{q}_c is a good first approximation.

Appendix E: Competition between z-BOP and superconductivity

We introduce the eight-spinor field

$$\psi_{\mathbf{k}}^{\dagger} = (f_{\mathbf{k}\uparrow,1}^{\dagger}, f_{\mathbf{k}\uparrow,2}^{\dagger}, f_{-\mathbf{k}\downarrow,1}, f_{-\mathbf{k}\downarrow,2}, f_{\mathbf{k}+\mathbf{q}_c\uparrow,1}^{\dagger}, f_{\mathbf{k}+\mathbf{q}_c\uparrow,2}^{\dagger}, f_{-\mathbf{k}-\mathbf{q}_c\downarrow,1}, f_{-\mathbf{k}-\mathbf{q}_c\downarrow,2}) \quad (\text{E1})$$

where \mathbf{q}_c is the ordered momentum of the z-BOP. The inverse of the 8×8 Green function can be written as

$$G^{-1}(\mathbf{k}, i\nu_n) = \begin{pmatrix} A & B \\ B & C \end{pmatrix}, \quad (\text{E2})$$

with A , B , and C the following 4×4 matrices

$$A = \begin{pmatrix} i\nu_n - \varepsilon_{\mathbf{k}}^{\parallel} & -\varepsilon_{\perp} & 0 & -\Delta_{\perp} \\ -\varepsilon_{\perp} & i\nu_n - \varepsilon_{\mathbf{k}}^{\parallel} & -\Delta_{\perp} & 0 \\ 0 & -\Delta_{\perp} & i\nu_n + \varepsilon_{\mathbf{k}}^{\parallel} & \varepsilon_{\perp} \\ -\Delta_{\perp} & 0 & \varepsilon_{\perp} & i\nu_n + \varepsilon_{\mathbf{k}}^{\parallel} \end{pmatrix}, \quad (\text{E3})$$

$$B = \begin{pmatrix} 0 & -\phi & 0 & 0 \\ -\phi & 0 & 0 & 0 \\ 0 & 0 & 0 & \phi \\ 0 & 0 & \phi & 0 \end{pmatrix}, \quad (\text{E4})$$

and C has the form of A with $\mathbf{k} + \mathbf{q}_c$ instead of \mathbf{k} . Δ_{\perp} and ϕ are the out-of-plane superconducting and z-BOP gap, respectively. The gap equations for Δ_{\perp} and ϕ are

$$\Delta_{\perp} = -\frac{J_{\perp}}{4} \sum_{\mathbf{k}, i\nu_n} G_{14}(\mathbf{k}, i\nu_n), \quad (\text{E5})$$

and

$$\phi = -\frac{J_{\perp}}{2} \sum_{\mathbf{k}, i\nu_n} G_{16}(\mathbf{k}, i\nu_n) \quad (\text{E6})$$

and must be solved self consistently.

-
- [1] H. Sun, M. Huo, X. Hu, J. Li, Z. Liu, Y. Han, L. Tang, Z. Mao, P. Yang, B. Wang, J. Cheng, D.-X. Yao, G.-M. Zhang, and M. Wang, Signatures of superconductivity near 80 K in a nickelate under high pressure, *Nature* **621**, 493 (2023).
- [2] J. Hou, P.-T. Yang, Z.-Y. Liu, J.-Y. Li, P.-F. Shan, L. Ma, G. Wang, N.-N. Wang, H.-Z. Guo, J.-P. Sun, Y. Uwatoko, M. Wang, G.-M. Zhang, B.-S. Wang, and J.-G. Cheng, Emergence of High-Temperature Superconducting Phase in Pressurized La₃Ni₂O₇ Crystals, *Chinese Physics Letters* **40**, 117302 (2023).
- [3] J. Yang, H. Sun, X. Hu, Y. Xie, T. Miao, H. Luo, H. Chen, B. Liang, W. Zhu, G. Qu, C.-Q. Chen, M. Huo,

- Y. Huang, S. Zhang, F. Zhang, F. Yang, Z. Wang, Q. Peng, H. Mao, G. Liu, Z. Xu, T. Qian, D.-X. Yao, M. Wang, L. Zhao, and X. J. Zhou, Orbital-dependent electron correlation in double-layer nickelate La₃Ni₂O₇, *Nature Communications* **15**, 4373 (2024).
- [4] M. Kakoi, T. Oi, Y. Ohshita, M. Yashima, K. Kuroki, T. Kato, H. Takahashi, S. Ishiwata, Y. Adachi, N. Hatada, T. Uda, and H. Mukuda, Multiband Metallic Ground State in Multilayered Nickelates La₃Ni₂O₇ and La₄Ni₃O₁₀ Probed by ¹³⁹La-NMR at Ambient Pressure, *Journal of the Physical Society of Japan* **93**, 10.7566/jpsj.93.053702 (2024).

- [5] H. Sakakibara, M. Ochi, H. Nagata, Y. Ueki, H. Sakurai, R. Matsumoto, K. Terashima, K. Hirose, H. Ohta, M. Kato, Y. Takano, and K. Kuroki, Theoretical analysis on the possibility of superconductivity in the trilayer Ruddlesden-Popper nickelate $\text{La}_4\text{Ni}_3\text{O}_{10}$ under pressure and its experimental examination: Comparison with $\text{La}_3\text{Ni}_2\text{O}_7$, *Phys. Rev. B* **109**, 144511 (2024).
- [6] F. Li, N. Guo, Q. Zheng, Y. Shen, S. Wang, Q. Cui, C. Liu, S. Wang, X. Tao, G.-M. Zhang, and J. Zhang, Design and synthesis of three-dimensional hybrid Ruddlesden-Popper nickelate single crystals, *Physical Review Materials* **8**, 10.1103/physrevmaterials.8.053401 (2024).
- [7] X. Chen, J. Zhang, A. S. Thind, S. Sharma, H. LaBollita, G. Peterson, H. Zheng, D. P. Phelan, A. S. Botana, R. F. Klie, and J. F. Mitchell, Polymorphism in the Ruddlesden-Popper Nickelate $\text{La}_3\text{Ni}_2\text{O}_7$: Discovery of a Hidden Phase with Distinctive Layer Stacking, *Journal of the American Chemical Society* **146**, 3640–3645 (2024).
- [8] P. Puphal, P. Reiss, N. Enderlein, Y.-M. Wu, G. Khalullin, V. Sundaramurthy, T. Priessnitz, M. Knauff, A. Suthar, L. Richter, M. Isobe, P. A. van Aken, H. Takagi, B. Keimer, Y. E. Suyolcu, B. Wehinger, P. Hansmann, and M. Hepting, Unconventional Crystal Structure of the High-Pressure Superconductor $\text{La}_3\text{Ni}_2\text{O}_7$, *Phys. Rev. Lett.* **133**, 146002 (2024).
- [9] Y. Zhou, J. Guo, S. Cai, H. Sun, P. Wang, J. Zhao, J. Han, X. Chen, Y. Chen, Q. Wu, Y. Ding, T. Xiang, H. Kwang Mao, and L. Sun, Evidence of filamentary superconductivity in pressurized $\text{La}_3\text{Ni}_2\text{O}_7$ (2024), arXiv:2311.12361 [cond-mat.supr-con].
- [10] Z. Liu, M. Huo, J. Li, Q. Li, Y. Liu, Y. Dai, X. Zhou, J. Hao, Y. Lu, M. Wang, and H.-H. Wen, Electronic correlations and partial gap in the bilayer nickelate $\text{La}_3\text{Ni}_2\text{O}_7$ (2024), arXiv:2307.02950 [cond-mat.supr-con].
- [11] Y. Zhang, D. Su, Y. Huang, Z. Shan, H. Sun, M. Huo, K. Ye, J. Zhang, Z. Yang, Y. Xu, Y. Su, R. Li, M. Smidman, M. Wang, L. Jiao, and H. Yuan, High-temperature superconductivity with zero-resistance and strange metal behavior in $\text{La}_3\text{Ni}_2\text{O}_{7-\delta}$ (2024), arXiv:2307.14819 [cond-mat.supr-con].
- [12] Q.-G. Yang, D. Wang, and Q.-H. Wang, Possible s_{\pm} -wave superconductivity in $\text{La}_3\text{Ni}_2\text{O}_7$, *Phys. Rev. B* **108**, L140505 (2023).
- [13] Q. Li, Y.-J. Zhang, Z.-N. Xiang, Y. Zhang, X. Zhu, and H.-H. Wen, Signature of Superconductivity in Pressurized $\text{La}_4\text{Ni}_3\text{O}_{10}$, *Chinese Physics Letters* **41**, 017401 (2024).
- [14] K. Chen, X. Liu, J. Jiao, M. Zou, Y. Luo, Q. Wu, N. Zhang, Y. Guo, and L. Shu, Evidence of spin density waves in $\text{La}_3\text{Ni}_2\text{O}_{7-\delta}$ (2024), arXiv:2311.15717 [cond-mat.str-el].
- [15] Y. Zhu, D. Peng, E. Zhang, B. Pan, X. Chen, L. Chen, H. Ren, F. Liu, Y. Hao, N. Li, Z. Xing, F. Lan, J. Han, J. Wang, D. Jia, H. Wo, Y. Gu, Y. Gu, L. Ji, W. Wang, H. Gou, Y. Shen, T. Ying, X. Chen, W. Yang, H. Cao, C. Zheng, Q. Zeng, J.-g. Guo, and J. Zhao, Superconductivity in pressurized trilayer $\text{La}_4\text{Ni}_3\text{O}_{10-\delta}$ single crystals, *Nature* **631**, 531 (2024).
- [16] T. Xie, M. Huo, X. Ni, F. Shen, X. Huang, H. Sun, H. C. Walker, D. Adroja, D. Yu, B. Shen, L. He, K. Cao, and M. Wang, Neutron Scattering Studies on the High- T_c Superconductor $\text{La}_3\text{Ni}_2\text{O}_{7-\delta}$ at Ambient Pressure (2024), arXiv:2401.12635 [cond-mat.supr-con].
- [17] X. Chen, J. Choi, Z. Jiang, J. Mei, K. Jiang, J. Li, S. Agrestini, M. Garcia-Fernandez, X. Huang, H. Sun, D. Shen, M. Wang, J. Hu, Y. Lu, K.-J. Zhou, and D. Feng, Electronic and magnetic excitations in $\text{La}_3\text{Ni}_2\text{O}_7$ (2024), arXiv:2401.12657 [cond-mat.supr-con].
- [18] Z. Dan, Y. Zhou, M. Huo, Y. Wang, L. Nie, M. Wang, T. Wu, and X. Chen, Spin-density-wave transition in double-layer nickelate $\text{La}_3\text{Ni}_2\text{O}_7$ (2024), arXiv:2402.03952 [cond-mat.supr-con].
- [19] S. N. Abadi, K.-J. Xu, E. G. Lomeli, P. Puphal, M. Isobe, Y. Zhong, A. V. Fedorov, S.-K. Mo, M. Hashimoto, D.-H. Lu, B. Moritz, B. Keimer, T. P. Devereaux, M. Hepting, and Z.-X. Shen, Electronic structure of the alternating monolayer-trilayer phase of $\text{La}_3\text{Ni}_2\text{O}_7$ (2024), arXiv:2402.07143 [cond-mat.supr-con].
- [20] G. Wang, N. N. Wang, X. L. Shen, J. Hou, L. Ma, L. F. Shi, Z. A. Ren, Y. D. Gu, H. M. Ma, P. T. Yang, Z. Y. Liu, H. Z. Guo, J. P. Sun, G. M. Zhang, S. Calder, J.-Q. Yan, B. S. Wang, Y. Uwatoko, and J.-G. Cheng, Pressure-Induced Superconductivity In Polycrystalline $\text{La}_3\text{Ni}_2\text{O}_{7-\delta}$, *Phys. Rev. X* **14**, 011040 (2024).
- [21] M. Zhang, C. Pei, X. Du, W. Hu, Y. Cao, Q. Wang, J. Wu, Y. Li, H. Liu, C. Wen, Y. Zhao, C. Li, W. Cao, S. Zhu, Q. Zhang, N. Yu, P. Cheng, L. Zhang, Z. Li, J. Zhao, Y. Chen, H. Guo, C. Wu, F. Yang, S. Yan, L. Yang, and Y. Qi, Superconductivity in trilayer nickelate $\text{La}_4\text{Ni}_3\text{O}_{10}$ under pressure (2024), arXiv:2311.07423 [cond-mat.supr-con].
- [22] Z. Luo, X. Hu, M. Wang, W. Wú, and D.-X. Yao, Bilayer two-orbital model of $\text{La}_3\text{Ni}_2\text{O}_7$ under pressure, *Phys. Rev. Lett.* **131**, 126001 (2023).
- [23] Y. Zhang, L.-F. Lin, A. Moreo, and E. Dagotto, Electronic structure, dimer physics, orbital-selective behavior, and magnetic tendencies in the bilayer nickelate superconductor $\text{La}_3\text{Ni}_2\text{O}_7$ under pressure, *Phys. Rev. B* **108**, L180510 (2023).
- [24] F. Lechermann, J. Gondolf, S. Bötzel, and I. M. Eremin, Electronic correlations and superconducting instability in $\text{La}_3\text{Ni}_2\text{O}_7$ under high pressure, *Phys. Rev. B* **108**, L201121 (2023).
- [25] H. Sakakibara, N. Kitamine, M. Ochi, and K. Kuroki, Possible high T_c superconductivity in $\text{La}_3\text{Ni}_2\text{O}_7$ under high pressure through manifestation of a nearly half-filled bilayer hubbard model, *Phys. Rev. Lett.* **132**, 106002 (2024).
- [26] Q.-G. Yang, D. Wang, and Q.-H. Wang, Possible s_{\pm} -wave superconductivity in $\text{La}_3\text{Ni}_2\text{O}_7$, *Phys. Rev. B* **108**, L140505 (2023).
- [27] Y. Gu, C. Le, Z. Yang, X. Wu, and J. Hu, Effective model and pairing tendency in bilayer Ni-based superconductor $\text{La}_3\text{Ni}_2\text{O}_7$ (2023), arXiv:2306.07275 [cond-mat.supr-con].
- [28] Z. Liao, L. Chen, G. Duan, Y. Wang, C. Liu, R. Yu, and Q. Si, Electron correlations and superconductivity in $\text{La}_3\text{Ni}_2\text{O}_7$ under pressure tuning, *Phys. Rev. B* **108**, 214522 (2023).
- [29] Q. Qin, J. Wang, and Y.-f. Yang, Frustrated Superconductivity in the Trilayer Nickelate $\text{La}_4\text{Ni}_3\text{O}_{10}$ (2024), arXiv:2405.04340 [cond-mat.supr-con].
- [30] H. Yang, H. Oh, and Y.-H. Zhang, Strong pairing from a small Fermi surface beyond weak coupling: Application to $\text{La}_3\text{Ni}_2\text{O}_7$, *Phys. Rev. B* **110**, 104517 (2024).
- [31] Q. Qin and Y.-f. Yang, High- T_c superconductivity by mobilizing local spin singlets and possible route to higher T_c in pressurized $\text{La}_3\text{Ni}_2\text{O}_7$,

- Phys. Rev. B **108**, L140504 (2023).
- [32] Y.-Y. Zheng and W. Wú, Superconductivity in the Bilayer Two-orbital Hubbard Model (2023), arXiv:2312.03605 [cond-mat.str-el].
- [33] C. Lu, Z. Pan, F. Yang, and C. Wu, Interplay of two E_g orbitals in Superconducting $\text{La}_3\text{Ni}_2\text{O}_7$ Under Pressure (2023), arXiv:2310.02915 [cond-mat.supr-con].
- [34] Z. Luo, B. Lv, M. Wang, W. Wú, and D.-X. Yao, High-TC superconductivity in $\text{La}_3\text{Ni}_2\text{O}_7$ based on the bilayer two-orbital t-J model, npj Quantum Materials **9**, 61 (2024).
- [35] C. Lu, Z. Pan, F. Yang, and C. Wu, Interlayer-Coupling-Driven High-Temperature Superconductivity in $\text{La}_3\text{Ni}_2\text{O}_7$ under Pressure, Phys. Rev. Lett. **132**, 146002 (2024).
- [36] X.-Z. Qu, D.-W. Qu, J. Chen, C. Wu, F. Yang, W. Li, and G. Su, Bilayer $t-J-J_\perp$ Model and Magnetically Mediated Pairing in the Pressurized Nickelate $\text{La}_3\text{Ni}_2\text{O}_7$, Phys. Rev. Lett. **132**, 036502 (2024).
- [37] H. Oh and Y.-H. Zhang, Type-II $t-J$ model and shared superexchange coupling from Hund's rule in superconducting $\text{La}_3\text{Ni}_2\text{O}_7$, Phys. Rev. B **108**, 174511 (2023).
- [38] K. Jiang, Z. Wang, and F.-C. Zhang, High-temperature superconductivity in $\text{La}_3\text{Ni}_2\text{O}_7$, Chinese Physics Letters **41**, 017402 (2024).
- [39] Y. Shen, M. Qin, and G.-M. Zhang, Effective Bilayer Model Hamiltonian and Density-Matrix Renormalization Group Study for the High-Tc Superconductivity in $\text{La}_3\text{Ni}_2\text{O}_7$ under High Pressure, Chinese Physics Letters **40**, 127401 (2023).
- [40] W. Wú, Z. Luo, D.-X. Yao, and M. Wang, Superexchange and charge transfer in the nickelate superconductor $\text{La}_3\text{Ni}_2\text{O}_7$ under pressure, Science China Physics, Mechanics & Astronomy **67**, 117402 (2024).
- [41] Y.-B. Liu, J.-W. Mei, F. Ye, W.-Q. Chen, and F. Yang, s^\pm -Wave Pairing and the Destructive Role of Apical-Oxygen Deficiencies in $\text{La}_3\text{Ni}_2\text{O}_7$ under Pressure, Phys. Rev. Lett. **131**, 236002 (2023).
- [42] Y.-f. Yang, G.-M. Zhang, and F.-C. Zhang, Interlayer valence bonds and two-component theory for high- T_c superconductivity of $\text{La}_3\text{Ni}_2\text{O}_7$ under pressure, Phys. Rev. B **108**, L201108 (2023).
- [43] Z. Luo, X. Hu, M. Wang, W. Wú, and D.-X. Yao, Bilayer Two-Orbital Model of $\text{La}_3\text{Ni}_2\text{O}_7$ under Pressure, Phys. Rev. Lett. **131**, 126001 (2023).
- [44] Z. Pan, C. Lu, F. Yang, and C. Wu, Effect of Rare-earth Element Substitution in Superconducting $\text{R}_3\text{Ni}_2\text{O}_7$ Under Pressure (2023), arXiv:2309.06173 [cond-mat.supr-con].
- [45] X.-Z. Qu, D.-W. Qu, W. Li, and G. Su, Roles of Hund's Rule and Hybridization in the Two-orbital Model for High- T_c Superconductivity in the Bilayer Nickelate (2023), arXiv:2311.12769 [cond-mat.str-el].
- [46] P.-F. Tian, H.-T. Ma, X. Ming, X.-J. Zheng, and H. Li, Effective model and electron correlations in trilayer nickelate superconductor $\text{La}_4\text{Ni}_3\text{O}_{10}$, Journal of Physics: Condensed Matter **36**, 355602 (2024).
- [47] J.-X. Wang, Z. Ouyang, R.-Q. He, and Z.-Y. Lu, Non-Fermi liquid and Hund correlation in $\text{La}_4\text{Ni}_3\text{O}_{10}$ under high pressure, Phys. Rev. B **109**, 165140 (2024).
- [48] J. Zhan, Y. Gu, X. Wu, and J. Hu, Cooperation between electron-phonon coupling and electronic interaction in bilayer nickelates $\text{La}_3\text{Ni}_2\text{O}_7$ (2024), arXiv:2404.03638 [cond-mat.supr-con].
- [49] M. Wang, H.-H. Wen, T. Wu, D.-X. Yao, and T. Xiang, Normal and superconducting properties of $\text{La}_3\text{Ni}_2\text{O}_7$ (2024), arXiv:2406.04837 [cond-mat.str-el].
- [50] M. Hepting, Nickelates join the club of high-temperature superconductors, Nature **621**, 475 (2023).
- [51] J. Li, P. Ma, H. Zhang, X. Huang, C. Huang, M. Huo, D. Hu, Z. Dong, C. He, J. Liao, X. Chen, T. Xie, H. Sun, and M. Wang, Pressure-driven right-triangle shape superconductivity in bilayer nickelate $\text{La}_3\text{Ni}_2\text{O}_7$ (2024), arXiv:2404.11369 [cond-mat.supr-con].
- [52] N. Wang, G. Wang, X. Shen, J. Hou, J. Luo, X. Ma, H. Yang, L. Shi, J. Dou, J. Feng, J. Yang, Y. Shi, Z. Ren, H. Ma, P. Yang, Z. Liu, Y. Liu, H. Zhang, X. Dong, Y. Wang, K. Jiang, J. Hu, S. Nagasaki, K. Kitagawa, S. Calder, J. Yan, J. Sun, B. Wang, R. Zhou, Y. Uwatoko, and J. Cheng, Bulk high-temperature superconductivity in pressurized tetragonal $\text{La}_2\text{PrNi}_2\text{O}_7$, Nature **634**, 579 (2024).
- [53] J. Wen, Y. Xu, G. Wang, Z.-X. He, Y. Chen, N. Wang, T. Lu, X. Ma, F. Jin, L. Chen, M. Liu, J.-W. Fan, X. Liu, X.-Y. Pan, G.-Q. Liu, J. Cheng, and X. Yu, Probing the meissner effect in pressurized bilayer nickelate superconductor (2024), arXiv:2410.10275 [cond-mat.supr-con].
- [54] B. Keimer, S. A. Kivelson, M. R. Norman, S. Uchida, and J. Zaanen, From quantum matter to high-temperature superconductivity in copper oxides, Nature **518**, 179 (2015).
- [55] T. Timusk and B. Statt, The pseudogap in high-temperature superconductors: an experimental survey, Reports on Progress in Physics **62**, 61 (1999).
- [56] S. M. Hayden and J. M. Tranquada, Charge correlations in cuprate superconductors, Annual Review of Condensed Matter Physics **15**, 215 (2024).
- [57] P. Proust and L. Taillefer, The remarkable underlying ground states of cuprate superconductors, Annual Review of Condensed Matter Physics **10**, 409 (2019).
- [58] C. Pépin, D. Chakraborty, M. Grandadam, and S. Sarkar, Fluctuations and the higgs mechanism in underdoped cuprates, Annual Review of Condensed Matter Physics **11**, 301 (2020).
- [59] P. A. Lee, N. Nagaosa, and X.-G. Wen, Doping a mott insulator: Physics of high-temperature superconductivity, Rev. Mod. Phys. **78**, 17 (2006).
- [60] R. H. McKenzie, Science **278**, 820 (1997).
- [61] K. Takada, H. Sakurai, E. Takayama-Muromachi, F. Izumi, R. A. Dilanian, and T. Sasaki, Superconductivity in two-dimensional CoO_2 layers, Nature **422**, 53 (2003).
- [62] D. J. Scalapino, A common thread: The pairing interaction for unconventional superconductors, Rev. Mod. Phys. **84**, 1383 (2012).
- [63] B. R. Ortiz, L. C. Gomes, J. R. Morey, M. Winiarski, M. Bordelon, J. S. Mangum, I. W. H. Oswald, J. A. Rodriguez-Rivera, J. R. Neilson, S. D. Wilson, E. Ertekin, T. M. McQueen, and E. S. Toberer, New kagome prototype materials: discovery of KV_3Sb_5 , RbV_3Sb_5 , and CsV_3Sb_5 , Phys. Rev. Mater. **3**, 094407 (2019).
- [64] N. M. R., Entering the nickel age of superconductivity, Physics **13**, 85 (2020).
- [65] F. C. Zhang and T. M. Rice, Effective Hamiltonian for the superconducting Cu oxides, Phys. Rev. B **37**, 3759 (1988).

- [66] A. Foussats, A. Greco, and O. Zandron, First-Order Lagrangians and Path-Integral Quantization in the t - J Model, *Annals of Physics* **275**, 238 (1999).
- [67] A. Foussats and A. Greco, Large- N expansion based on the Hubbard operator path integral representation and its application to the t - J model. II. The case for finite J , *Phys. Rev. B* **70**, 205123 (2004).
- [68] J. Hubbard, Electron correlations in narrow energy bands, *Proc. R. Soc. Lond. A: Mathematical, Physical and Engineering Sciences* **276**, 238 (1963).
- [69] H. Yamase and W. Metzner, Magnetic excitations and their anisotropy in $\text{YBa}_2\text{Cu}_3\text{O}_{6+x}$: Slave-boson mean-field analysis of the bilayer t - J model, *Phys. Rev. B* **73**, 214517 (2006).
- [70] L. Zinni, M. Bejas, and A. Greco, Superconductivity with and without glue and the role of the double-occupancy forbidding constraint in the t - J - V model, *Phys. Rev. B* **103**, 134504 (2021).
- [71] P. W. Anderson, Is There Glue in Cuprate Superconductors?, *Science* **316**, 1705 (2007), <https://www.science.org/doi/pdf/10.1126/science.1140970>.
- [72] T. A. Maier, D. Poilblanc, and D. J. Scalapino, Dynamics of the Pairing Interaction in the Hubbard and t - J Models of High-Temperature Superconductors, *Phys. Rev. Lett.* **100**, 237001 (2008).
- [73] H. Yamase, M. Bejas, and A. Greco, Plasmarons in high-temperature cuprate superconductors, *Communications Physics* **6**, 168 (2023).
- [74] M. Bejas, A. Greco, and H. Yamase, Possible charge instabilities in two-dimensional doped Mott insulators, *Phys. Rev. B* **86**, 224509 (2012).
- [75] I. Affleck and J. B. Marston, Large- n limit of the Heisenberg-Hubbard model: Implications for high- T_c superconductors, *Phys. Rev. B* **37**, 3774 (1988).
- [76] E. Cappelluti and R. Zeyher, Interplay between superconductivity and flux phase in the t - J model, *Phys. Rev. B* **59**, 6475 (1999).
- [77] D. C. Morse and T. C. Lubensky, Instabilities of the Fermi-liquid and staggered flux phases in the large- N t - J model, *Phys. Rev. B* **43**, 10436 (1991).
- [78] S. Chakravarty, R. B. Laughlin, D. K. Morr, and C. Nayak, Hidden order in the cuprates, *Phys. Rev. B* **63**, 094503 (2001).
- [79] W.-L. Tu and T.-K. Lee, Genesis of charge orders in high temperature superconductors, *Scientific Reports* **6**, 18675 (2016).
- [80] S. Ghosh, T. C. Lubensky, T.-K. Lee, and P. J. Hirschfeld, Incommensurate charge ordered states in the t - t' - j model, *New Journal of Physics* **19**, 013028 (2017).
- [81] D. Chakraborty, M. Grandadam, M. H. Hamidian, J. C. S. Davis, Y. Sidis, and C. Pépin, Fractionalized pair density wave in the pseudogap phase of cuprate superconductors, *Phys. Rev. B* **100**, 224511 (2019).
- [82] R. Zeyher and A. Greco, Competition between superconductivity and the pseudogap phase in the t - J model, *physica status solidi (b)* **236**, 343 (2003).
- [83] H. Oh, B. Zhou, and Y.-H. Zhang, Type II t - J model in charge transfer regime in bilayer $\text{La}_3\text{Ni}_2\text{O}_7$ and trilayer $\text{La}_4\text{Ni}_3\text{O}_{10}$ (2024), arXiv:2405.00092 [cond-mat.str-el].
- [84] Note that we have to use 1eV for t because the $1/N$ scaling in the large- N expansion [67].
- [85] L. Craco and S. Leoni, Strange metal and coherence-incoherence crossover in pressurized $\text{La}_3\text{Ni}_2\text{O}_7$, *Phys. Rev. B* **109**, 165116 (2024).
- [86] G. Kotliar and J. Liu, Superconducting Instabilities in the Large- U Limit of a Generalized Hubbard Model, *Phys. Rev. Lett.* **61**, 1784 (1988).
- [87] J. C. Le Guillou and E. Ragoucy, Slave-particle quantization and sum rules in the t - j model, *Phys. Rev. B* **52**, 2403 (1995).
- [88] H. Yamase, M. Bejas, and A. Greco, Electron self-energy from quantum charge fluctuations in the layered t - J model with long-range Coulomb interaction, *Phys. Rev. B* **104**, 045141 (2021).